



Data mining in photocatalytic water splitting over perovskites literature for higher hydrogen production

Elif Can, Ramazan Yildirim*

Department of Chemical Engineering, Bogazici University, Istanbul, 34342, Turkey



ARTICLE INFO

Keywords:

Photocatalytic water splitting
Perovskite semiconductor
Band gap modification
Machine-learning
Data mining

ABSTRACT

A database containing 540 cases from 151 published papers on photocatalytic water splitting over perovskites was constructed and analyzed using data mining tools; the factors leading high hydrogen production were identified by association rule mining while some useful heuristics for the future studies were developed by decision tree analysis. Additionally, the predictive models were developed using random forest regression.

In about half of the works, the perovskites were doped by A-site, B-site or both; however, only some portion of doped catalysts had better activity than plain perovskites while doping also improved stability in some cases. The effect of co-catalyst on activity seems to be also irregular; no definitive conclusion could be drawn. The effects of preparation methods on surface area, band gap and crystal structure were noticeable. This is also observed in visible light activity; for example the materials prepared by hydrothermal synthesis method appeared to perform better under visible light. Methanol and other sacrificial agents were used in both UV and visible light tests while inorganic additives have been commonly utilized under visible light. The band gap was found to be highly predictable but it could not be directly linked to the hydrogen production. As the result, although there has been significant progress in the field, the improvement in hydrogen production appeared to be always limited; the sound solutions like ion doping to modify the band gap, use of co-catalyst for charge separation or use of additives as sacrificial agents did not to help as much as desired.

1. Introduction

Hydrogen is considered as a promising energy carrier due to its high energy density, abundance in nature and cleanness; it can be used as a fuel or utilized in synthetic fuel production through Fisher-Tropsch type processes. However, the hydrogen is mostly produced via steam reforming or partial oxidation of fossil fuels (natural gas is the largest resource with 48%) [1,2]. Since these processes significantly contribute to the greenhouse gas emissions, new and cleaner technologies like semiconductor based solar water splitting have been extensively studied in recent years. The ultimate goal is to use solar energy, which is clean, renewable and free of charge.

Fujishima and Honda split water under UV as the first time in 1972; they used a photoelectrochemical cell made of a semiconductor photoanode, cathode and electrolyte solution [3]. A few years later, the studies on photocatalytic water splitting (PWS) over particulate semiconductors also started [4]. More than 140 materials have been used as semiconductor [5]. TiO_2 is the first, and still the most common semiconductor due to its low cost, stability, nontoxicity and environmental-friendliness [4,6]. However, its band gap is suitable for UV light, which

is only 4% of sunlight [7]; it has to be modified by ion doping and sensitization for the visible light (43% of sunlight). Perovskites have also gained significant attention in recent years because they can be not only synthesized in numerous formulations and structures, but also easily modified by various methods.

The recombination of photo-excited electrons and holes before splitting water is a big challenge for PWS, and co-catalysts (or promoters) were used to inhibit this [8]; Pt, Ru, Ir, NiO_x and Rh are the most common co-catalysts. Methanol, ethanol or some other sacrificial agents are also added to the reaction solution to suppress back reaction.

Existence of numerous options for materials and methods constitutes a large domain for PWS research. Consequently, large number of papers has been published in recent years creating a massive accumulation of experience in literature. However, this accumulation cannot be effectively utilized with conventional approaches because it is too big, heterogeneous and distributed among the large number of sources. Instead, the machine learning and data mining tools, which were developed to extract non-trivial, previously unknown, and potentially useful knowledge from large and complex databases, can be used for this purpose. These tools have been implemented in numerous

* Corresponding author.

E-mail address: yildirra@boun.edu.tr (R. Yildirim).

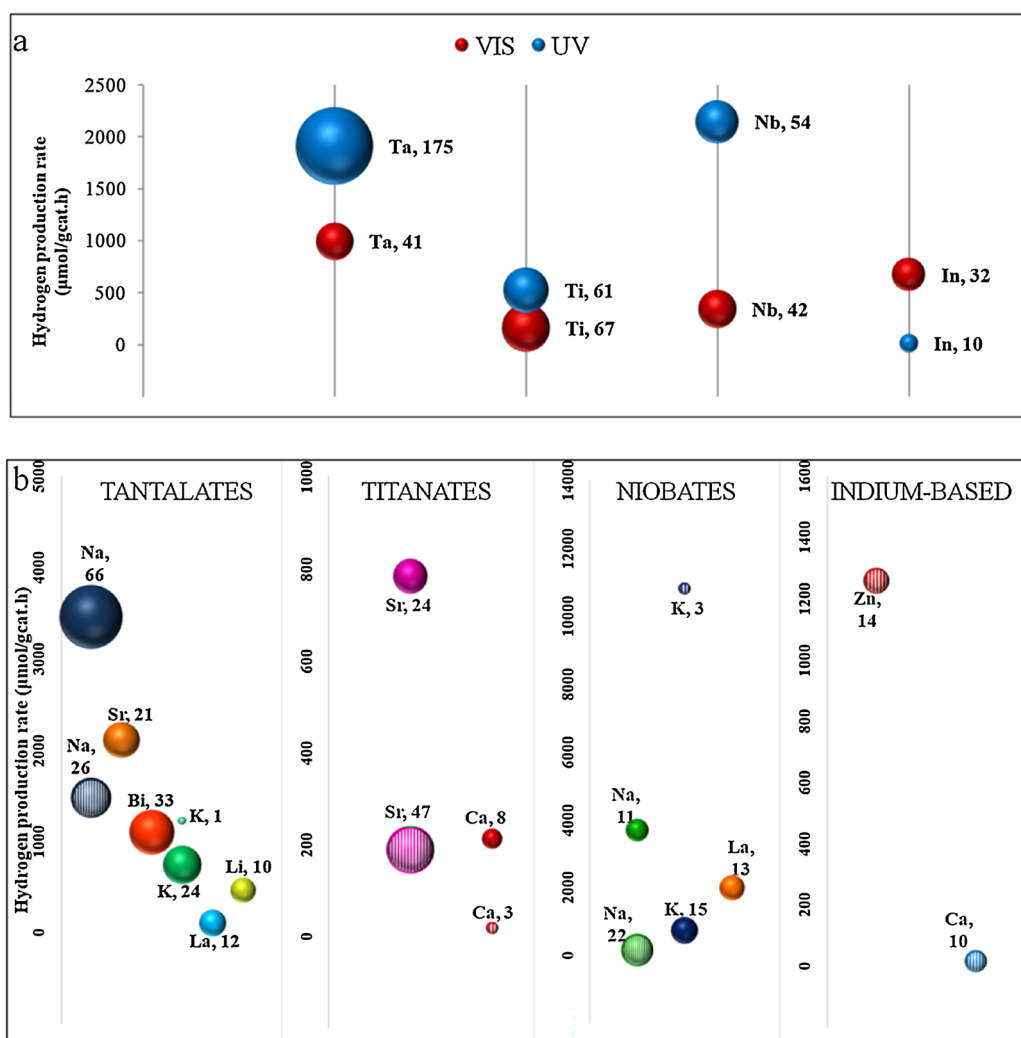


Fig. 1. Average hydrogen production rates based on a) common B-site elements and b) common A-site elements (solid balls are for UV; dashed balls are for visible light).

subjects from economy and health to astronomy and biology in recent years. Additionally, some groups (including ours) constructed and analyzed databases from past publications on catalytic CO oxidation [9], water gas shift reaction [10], steam and CO₂ reforming of methane [11,12], direct alcohol fuel cells [13], photocatalysis over titania [14] oxidative coupling of methane [15]. There are also works reporting the simultaneous use of molecular modeling and machine learning; the examples are study of structure-activity relationship for CO adsorption over Au clusters [16], screening of perovskites for thermochemical water splitting [17] and predicting the crystal structure of materials [18].

In this work, an extensive database for PWS over perovskites was constructed and analyzed using simple descriptive statistics together with a review of literature (works involving photoelectrochemical cells or organolead perovskites, which are used in solar cells, were not included). Then the database was examined in more details using data mining tools, which are suitable to analyze the perovskite semiconductors with numerous modifications and large structural differences. The association rule mining was used to determine the effects of most common factors while decision tree was used to develop selection rules and heuristics for high performance; the random forest technique was utilized to test the predictability of hydrogen production rate. The models to predict the band gap, which is often modified for visible light, were also constructed.

2. Methodology

2.1. Constructing database

The database was constructed from 151 experimental papers on PWS over perovskites published in 2005–2017; online sources including Elsevier, Wiley Online Library, American Chemical Society and Royal Society of Chemistry were reviewed (top hits in relevance sorting) and 540 instances (216 for visible; 324 for UV light) were extracted to form the database, which is given in Supplementary Material.

2.2. Computational details

The materials and methods used for photocatalyst preparation, properties of photocatalysts, and properties of reaction medium and light sources were used as input (predictor) variables while the hydrogen production rate was used as the output.

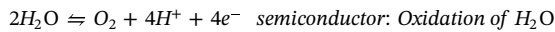
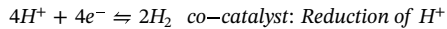
Datasets for visible and UV light were analyzed separately because their hydrogen production rates are different. For association rule mining and decision tree classification, each dataset was categorized in three classes as *low*, *medium* and *high* hydrogen production rates. The 4-fold cross validation was applied in decision tree and random forest analysis. All models were developed in RStudio; *apriori* algorithm in *arules* [19] package was used for association rule mining while *rpart* [20] and *randomForest* [21] were used for classification trees and

random forest respectively.

The complete list of variables with their ranges and the further details for computations are presented in Supplementary Material.

3. Review and pre-analysis of database

PWS reaction proceeds in three main steps: (i) absorption of photons and generation of electron and hole pairs, (ii) migration of electron to co-catalyst resulting in charge separation and (iii) surface reactions between these carriers to split water [22]. The mechanism of PWS can be described as follows:



The standard Gibbs free energy change is 237 kJ mol⁻¹ or 1.23 eV. The co-catalyst is not always required; some semiconductors provide active sites for hydrogen and oxygen evolution themselves; however, in most works, hydrogen was produced over co-catalyst while the semiconductor provides active site for oxygen evolution.

To develop an efficient photocatalyst, several parameters such as crystal structure, particle size, surface area and band gap energy of semiconductor have to be controlled; the type and loading of promoter, the contents of reaction solution and the characteristics of light source also affect the hydrogen yield [5].

3.1. Perovskite materials

The perovskites are the metal oxides with the general formula of ABX₃; A and B symbolize large and small cation respectively while X usually denotes oxygen (or occasionally halogens and S). The classification of perovskites by B-site is a common practice and it is also suitable for PWS [23,24]. The hydrogen evolution performances of most common perovskites (based on B-sites) are given in Fig. 1.a. The bubble sizes (and nearby numbers) indicate the frequency of perovskites in database containing those materials in their B-sites while the y-axis represents their average hydrogen evolution rate. The data obtained with UV (blue balls) and visible (red balls) light are presented separately. Since the number of data points in database is sufficiently large, the analyses presented below should represent the entire literature reasonable well.

Tantalates (Ta in B-site) are the most common perovskites in database; about 40% of data (216 of 541 cases) were in this class. They are followed by titanates (Ti containing), which forms 24% data (128 cases), niobates (Ni containing), which constitutes 18% of data (96 cases) and indium containing perovskites (8% corresponding to 42 cases). As expected, the hydrogen production rates are higher under UV. The tantalates and niobates perform much better under UV while the visible light performance of tantalates is also high. The average visible light activity of In catalysts is higher than their average UV performance because S containing perovskites (Al₂S₃) are used for visible light while Al₂O₃ are used under UV.

Fig. 1.b shows the frequency and performance of the most common perovskites according to A-sites; only perovskites having more than 10 cases with same A are presented in Fig. 1.b for better generalizations. If A and B sites are brought together, it can be easily seen that the most common five perovskites are NaTaOs (92 cases), SrTiOs (71 cases), BiTaOs (33 cases), NaNbOs (33 cases) and KTaOs (25 cases). Here, ABO symbolizes the general structure (not stoichiometric formula) including all bare and doped ABO₃ as well as the layered perovskites. More than two third of NaTaOs (66 of 92 points) were tested under UV, and resulted much higher average hydrogen production rate than that under visible light. For SrTiOs, however, 47 of 71 cases were obtained under visible light (only 24 UV cases). No visible light data was available for BiTaOs while NaNbOs were investigated under both UV (11 cases) and visible light (22 cases).

NaTaOs are not only the most common but also one of the most effective perovskites in the database (Fig. 1.b). As the most common material of the group, NaTaOs has a cubic crystal structure, which is believed to generate nano-step morphology and enhances the hydrogen production [24,25] while its high crystallinity improves PWS by inhibiting electron-hole recombination [25]. Additionally, its high surface area contributes to PWS activity by increasing active sites [25]. Their bond angle of 160°–180° may be also increasing the effectiveness of tantalates because the ideal bond angle of B–O–B in perovskite was found to be 180°, which is the best for its luminescent property [24,26,27]. SrTaOs, BiTaOs and KTaOs follow NaTaOs in hydrogen production with decreasing order. These perovskites have been also modified with ion doping [5,28,29], use of co-catalyst [5,28–31] and modifying the preparation methods [25,32] as discussed below.

SrTiOs are overwhelmingly the most common (55%) titanates in PWS; although their performances are not comparable to NaTaOs, they were frequently studied probably because Ti is more abundant. Besides, the band gap, surface area, particle size and crystallinity of SrTiOs can be easily tuned [33]. For example, Puangpitch et al. obtained a red-shift in absorption spectra of SrTiOs with co-catalysts like Au, Ag, Pt, Ni, Fe, and Ce and enhanced hydrogen yield (Au was the best) under UV [34]. Au/SrTiOs was also found to be effective (under visible light) by Saadetnejad and Yildirim [35]. CaTiOs, ZnTiOs, SnTiOs, KTiOs, BiTiOs and less common titanates like A₂Ti₂O₇ (A = Ga, La, Y) [36] were also investigated. Inserting nitrogen to oxygen site of ATiOs was also tested by Naik et al. with a red-shift in absorption spectrum [37].

As tantalates, the niobates also have high conduction band levels, which were reported to improve hydrogen production by facilitating reduction [24,25,29]. The band gaps of niobates were lower than those of tantalates; hence, they are more suitable for visible-light harvesting [24]. Na is the most frequently used A-site element even though the hydrogen production rates over KNbOs and LaNbOs are higher. The indium based photocatalysts also have considerable hydrogen production rates although the number of articles involving this class is rather limited. ZnInS₂ are the most common (and effective) In perovskites in database with low toxicity, high visible-light activity and stability. For example Li et al., synthesized and tested ZnIn_{1.5}S_{3.2575}, which kept its activity for 150 h; Ag doping to A-site (up to certain loading) further improved the activity under visible light [38]. These results were also verified over ZnIn_{2.3}S₄ [39].

3.2. Ion doping for band gap modification

Ion doping is a common and effective way to tune the band gap of perovskites. Doping changes the valence or conduction bands so that visible light harvesting may be possible [23]. Borgarello et al. studied ion doping in 1982 for the first time, and found that Cr doped TiO₂ produced more hydrogen under visible light than bare TiO₂ [23]. Since then, the metal and non-metal doping to semiconductors have been extensively studied. Indeed, 260 data points out of 540 (48%) in database were obtained over doped perovskites (31% A-site, 27% B-site). There were also works involving both A and B sites doping (about 10%) and doping one site with two elements; X-site doping (for oxygen) were also recorded.

3.2.1. A-site doping

For A-site doping, 18 elements were identified in the database; La (38 times) and Ca (32 times) were the most common elements followed by H (20 times), K (13 times), Br and Sr (10 times each). Ca, La, K, and H were the most frequent choices for tantalates; for example, 25 out of 32 cases of Ca doping involved tantalates while each of La, K and H appeared 12 times. However, La was overwhelmingly the most preferred element (20 times in database) for titanates while the other dopants were rarely used. H, Ca and La doped niobates were almost equally present (8, 7 and 6 times respectively); we had only Ag doping examples for In perovskites. Further details for the doping to common

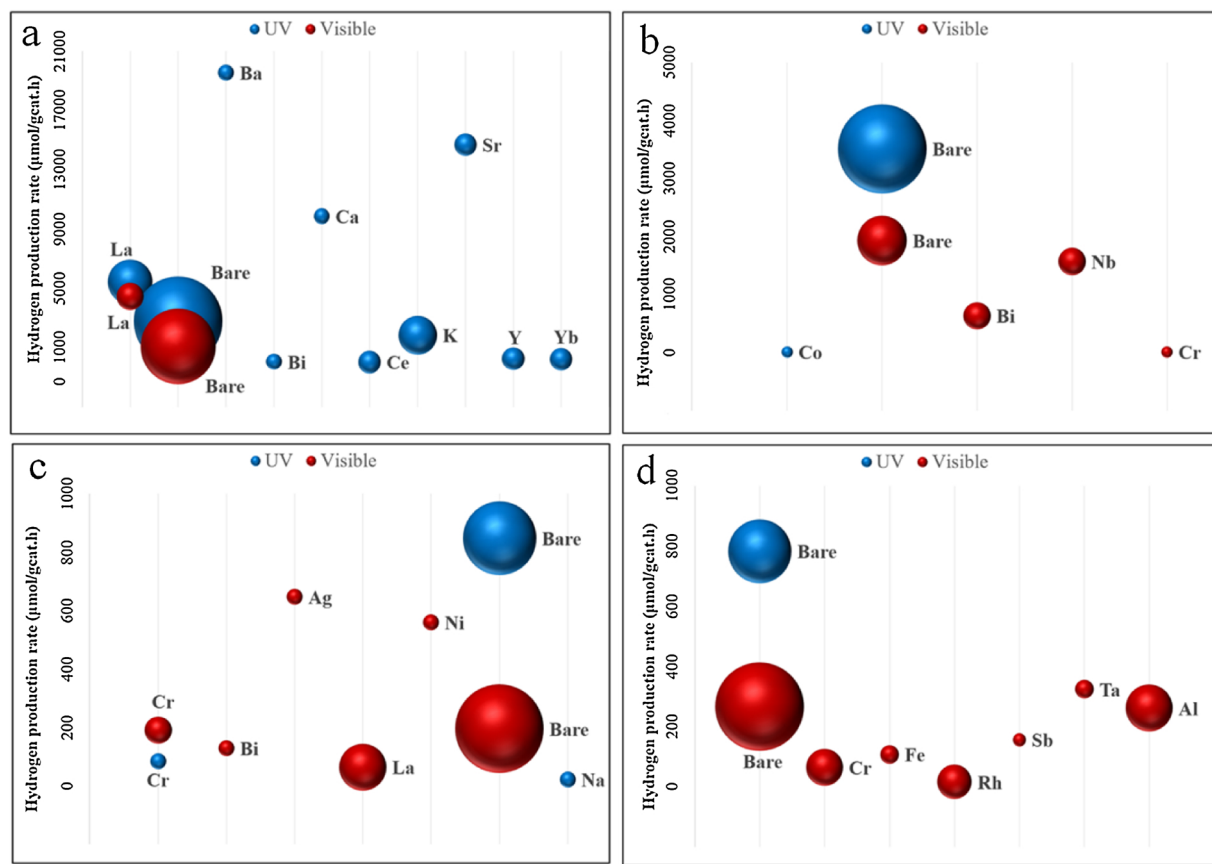


Fig. 2. The frequencies and average hydrogen production rates for a) A-site doped NaTaOs, b) B-site doped NaTaOs c) A-site doped SrTiOs, and d) B-site doped SrTiOs.

perovskites are given in Supplementary Material.

Although NaTaOs are the most effective photocatalysts for PWS, they lose their activity fast; hence, they are usually doped to suppress deactivation. About 30% of NaTaOs (28 out of 92) were doped in A-site with La and K or other less frequent elements. Various investigators reported that nickel co-catalyst and La dopant, together or separately, decreased electron-hole recombination and prolonged life of NaTaOs by creating new active sites [29,40–43]. Doping generally expands surface area (more active sites) and decreases particle size (shorter distance for photogenerated electrons to travel). For example, $\text{La}_x\text{Na}_y\text{TaO}_3$ resulted in much higher hydrogen production rate than bare NaTaO_3 under UV light [40–43]. Kudo et al. and Kato et al. also observed that solid-state reaction method created unique step structures on $\text{La}_x\text{Na}_y\text{TaO}_3$ particles and promoted hydrogen yield by generating new active sites [40,41]. The same group also studied Ca, Ba and Sr doped NaTaO_3 perovskites and obtained similar results [29]. Jana et al. doped rare elements (Y, La, Ce, and Yb) on NaTaO_3 , and found that Y: NaTaO_3 and La: NaTaO_3 had best performances (Y: NaTaO_3 was better) [44]. The performances of A-site doped NaTaOs are shown in Fig. 2.a as an example. La doping slightly improved average UV and visible light performances; however, Ba and Ca were more effective. The performance with other dopants was close to that of bare NaTaOs.

The other tantalates are also doped frequently. For example almost 50% of BiTaOs, the second most common tantalates, were mostly doped with Ba, Ca, and K; however, only the less frequently used Sr produced better result than undoped BiTaOs [45]; the average performances of Ba, Ca and K doped and undoped BiTaOs were almost the same.

Double metal or nonmetal doping to tantalates were also investigated. For example, Takayama et al., tested $\text{KCaSrTa}_5\text{O}_{15}$ with several promoters (NiO, Ni, Cu, Ru, Rh, Ag, Pt, and Au), and obtained the highest performance with NiO under UV [46]; Chen et al. reached

to a similar result over $\text{K}_{0.5}\text{La}_{0.5}\text{Bi}_2\text{Ta}_2\text{O}_9$ [47]. Shimizu et al. compared the activity of $\text{H}_2\text{La}_{2/3}\text{Ta}_2\text{O}_7$, $\text{K}_2\text{La}_{2/3}\text{Ta}_2\text{O}_7$, and $\text{H}_2\text{SrTa}_2\text{O}_7$ with KTaO_3 ; H doping improved hydrogen production by facilitating the transfer of photogenerated electrons and holes [48]. Similarly Huang et al. compared the efficiency of $\text{HSr}_2\text{TaNb}_2\text{O}_{10}$ with the perovskites doped with K; although they had nearly the same surface area, band gap and interlayer distance, H-doped perovskites provided better production rates [49].

A-site doping for SrTiOs was generally used to make these perovskites visible light active. However, the doping seemed to fail to improve activity in average; only few examples involving Ag and Ni produced better results than bare perovskites (Fig. 2.c). For example, Ag doping produced the hydrogen production rate of $648 \mu\text{mol gcat}^{-1} \text{h}^{-1}$ compared to the average of $243 \mu\text{mol gcat}^{-1} \text{h}^{-1}$ for bare SrTiO_3 [50]. However, La doping, which appeared in nine cases from three articles [51–53] in database, did not produce the same improvement. In one of these works [51], Luo et al. doped La to A-site of SrTiO_3 and obtained the hydrogen production rate of $67 \mu\text{mol gcat}^{-1} \text{h}^{-1}$; the other two groups [52,53] were also doped Cr in B site but they could not obtain improvement either. The hydrogen production rate over Cr [54] and Na [55] doped SrTiO_3 was also lower than the bare catalyst under UV.

The other titanates were also doped by their A-sites. For example, Li et al. synthesized Sn:KTiO and achieved a red shift in absorbance spectrum (the band gap was 2.8 eV while it was 3.5 eV for bare KTiO); the average hydrogen production rate was $257 \mu\text{mol gcat}^{-1} \text{h}^{-1}$ [56]. A-site of NaTiO_3 was also doped with La and its performance was compared with La and Cr co-doped (A and B site) NaTiO perovskite [57]. La: NaTiO did not result in significant hydrogen production rate; however, unlike to La, Cr: SrTiO discussed above [52,53], a sharp increase in the hydrogen production rate was observed when Cr is co-

doped to B site of La:NaTiO_3 .

It was difficult to make generalization for the A-site doping for niobates because the number of cases are limited (12 out of 96) while the number of dopants are high (nine different elements) in the database. The notable ones are H doping to SrNbO_3 and LaNbO_3 [58,59] and Ca doping to NaNbO_3 , BiNbO_3 , $\text{Co}_x\text{Nb}_y\text{O}_3$, and InNbO_3 perovskites [46,58,59]. $\text{H}_{2.33}\text{Sr}_{0.67}\text{Nb}_{5}\text{O}_{14.335}$ performed better than $\text{H}_2\text{LaNb}_2\text{O}_7$ (even better than H-In co-doped LaNbO_3) under UV. In both of those works [58,59], Pt was used as promoter, and their band gap values are similar to each other but $\text{H}_{2.33}\text{Sr}_{0.67}\text{Nb}_{5}\text{O}_{14.335}$ had larger surface area, which may be the reason of its better activity. In another work, Yin et al. tested Ca, Sr, and Ba doping to $\text{In}_{0.5}\text{Nb}_{0.5}\text{O}_3$ and $\text{Co}_{1/3}\text{Nb}_{2/3}\text{O}_3$ under UV in two separate articles [60,61]; the performances of doping agent were in the order of $\text{Ca} > \text{Sr} > \text{Ba}$ for InNbO_3 while the order were as $\text{Ba} > \text{Ca} > \text{Sr}$ for $\text{Co}_x\text{Nb}_y\text{O}_3$. Li et al. prepared Ca, Sr, Ba, and $\text{K}_{0.5}\text{La}_{0.5}$ doped $\text{Bi}_2\text{Nb}_2\text{O}_9$, and observed a red-shift in the doped catalysts compared to bare $\text{Bi}_2\text{Nb}_2\text{O}_9$. Sr-doped catalyst was the best while Ca and Ba-doped had worse performances under UV [62].

3.2.2. B-site doping

Examples containing 16 metals and transition metals doped for B-site were recorded in database. Doping of transition metal was reported to change donor-acceptor levels of perovskites so that band gap tuning was possible [23]. The tantalates were mostly doped by Nb (16) while Cr (18 cases) and Al (13 cases) doping were more common in titanates. The dominant choice for niobates was In with 16 cases even though Al, Ta and Zr were also used. Indium containing catalysts were B-doped less frequently (only 7 out of 42 data points).

NaTaOs were the most commonly B-doped tantalates in the database. For example, Bi doped Pt/NaTaO_3 was investigated by two groups in 2012. Kang et al. prepared Pt/Bi:NaTaO_3 by spray pyrolysis method while Kanhere et al. used solid state reaction (SSR) [63,64]. The former group claimed that unique surface morphology and large surface area increased the photocatalytic activity under visible light. The latter group, however, observed that their synthesis condition increased hydrogen yield by narrowing the band-gap [63,64]. Wang et al. doped Nb to B-site of NaTaO_3 at various ratios [65], and $\text{NaNb}_{0.5}\text{Ta}_{0.5}\text{O}_3$ showed 3.8 times higher hydrogen production than bare NaTaO_3 under visible light; this difference attributed to the lower band gap and defects generated by Nb. However, despite of these positive results, the average performance of Bi and Nb doped NaTaOs were worse than the bare perovskites (Fig. 2.b); this was also true for the other dopants.

B doping was also applied to other tantalates. For example, Huang et al. produced $\text{HSr}_2\text{TaNb}_2\text{O}_{10}$ with SSR and obtained 11 times higher hydrogen production rate than TiO_2 . They argued that $\text{HSr}_2\text{TaNb}_2\text{O}_{10}$ possessed a stable and special structure, which enabled separation of photogenerated electron-hole pairs [49]. Senthil et al. studied Bi (A-site) and Ce (B-site) doped SrTaO_3 , and found that, with Bi^{3+} and Ce^{4+} doping, the dipole moment was created; this improved the photocatalytic activity by enhancing charge separation [66]. Li et al. prepared $\text{La}_2\text{AlTaO}_7$ by SSR and studied under UV; Al doping lowered the conduction band, and the hydrogen production was succeeded even without a co-catalyst [67]. Zhang et al. prepared $\text{BiTa}_{1-x}\text{Cu}_x\text{O}_4$ with different amount of Cu [68]; the best performance under UV light was obtained over $\text{BiTa}_{0.98}\text{Cu}_{0.02}\text{O}_4$. Since all particles showed similar light diffuse reflectance spectra, the differences in activity was attributed to surface area change [68]. Ishihara et al., investigated the effects of Zr doping to KTaO_3 , and obtained much higher activity than bare KTaO_3 under UV [69].

SrTiO_3 is the most commonly B-doped perovskites, not only in titanates but also in the entire database (33 data points out of 71). Asai et al., studied Rh-doped and Rh-Sb co-doped SrTiO_3 in the presence of Ir co-catalyst, and they obtained the highest hydrogen yield over $\text{Rh}_{x}\text{Sb}_{y}\text{SrTiO}_3$ under UV. They argued that the doped metal ions worked as recombination centers unless another metal cation was co-doped to maintain the charge balance [70]. Recently, Ham et al. synthesized

Al:SrTiO_3 by flux-mediated method and SSR. For pure SrTiO_3 , the higher surface areas and enhanced crystallinity were obtained by flux-mediated method; the activity was also more than that obtained with SSR. However, in both case, the activity first increased with the increasing Al loading and then decreased with further increase of Al content [71]. Luo and Maggard synthesized Fe doped SrTiO_3 with hydrothermal method (HT); however they obtained no significant improvement compared to the bare SrTiO_3 [72].

Co-doping of two elements to A and B sites of SrTiO_3 was also tested; Kang et al. co-doped Ta to B-site and Cr or Ni to A-site; they obtained very large surface area and unique surface morphology that enhanced the photocatalytic activity under visible light (Ni gave better result); it was attributed that Ni and Ta ions created a charge balance around Ti, and made the surface morphology more suitable for PWS [73,74]. In another work, Kato and Kudo studied Cr doping to A-site and Sb doping to B-site of SrTiO_3 ; they achieved much higher visible light activity than those over single doped or undoped catalysts [75]. However, despite all these examples, the overall average performances of B doped SrTiO_3 were not better than plain perovskite (Fig. 2d).

The B-site doping was also implemented to other titanates. Huerta-Flores et al. observed an improvement in the activity of Zr doped $\text{Na}_2\text{Ti}_6\text{O}_{13}$ compared to bare catalyst, and attributed this to the different bond lengths and charge distribution of doped and bare samples; they also argued that Zr acted as an electron trap, which inhibited the recombination of electron-hole pairs [76]. Wang et al. and Lu et al. synthesized La,Cr co-doped CaTiO_3 , and both observed red shift in the band gap making this perovskite suitable for visible light [77,53].

The niobates were also B-doped (but less frequently than tantalates and titanates). For example, Lv et al. produced In doped NaNbO_3 particles with co-precipitation and observed surface area increase; however, the hydrogen production showed a plateau behavior indicating that improvement may be due to the better charge separation, not the surface area [78]. Iwakura et al. doped B-site of SrNbO_3 by Al, and changed the ordered and disordered material ratio in $\text{SrAl}_{0.5}\text{Nb}_{0.5}\text{O}_3$ by changing calcination time; the disordered $\text{SrAl}_{0.5}\text{Nb}_{0.5}\text{O}_3$ gave better hydrogen production rates under UV than ordered perovskites [79]; Li et al. investigated Cu doping to LaNiO_3 ; they claimed that Cu doping created a redox cycle of $\text{Cu}^{2+}/\text{Cu}^+$ over the pre-reduced Cu:LaNiO_3 , and promoted photocatalytic activity. They also found that pre-reduction treatment affected activity by changing electron-hole recombination rate, interfacial charge transfer and electronic structure [80,81].

Co-doping in niobates was also investigated. For example Li et al. co-doped La on A-site and Al on B-site of Bi_2NbO_7 [82]; they observed that La doping enhanced the activity under UV by changing electronic structure and optical absorption. Similarly, Wei et al. compared the performances of co-doped; they observed that $\text{H}_{x}\text{In:LaNbO}_3$ was one of the best due to its larger surface area and lower band gap [59]. In another work, Li et al. studied $\text{ALaTa}_{x/3}\text{Nb}_{2-x/3}\text{O}_7$ ($\text{A}=\text{K, H}$; $x=0, 2, 3, 4$ and 6), and obtained the best performance over $1\% \text{Pt/HLaTa}_{2/3}\text{Nb}_{4/3}\text{O}_7$. They claimed that Ta caused a new and more stable HLaNb_2O_7 form and created an electronic structure that helped the separation of photo-generated electron-hole pairs [83].

3.2.3. Doping effects on band gap

As presented above, there are numerous successful applications of doping in the literature; however, the average performance does not change significantly for most dopants. This can happen only if there are both high and low performances with the same dopant indicating that the other factor may be inflating or overshadowing the doping effects. In successful applications, the improvements were usually attributed to the shift in band gap, increase in surface area and decrease in particle size. Consequently, the effects of doping on these properties (if there are any) were also analyzed. No definitive conclusion could be drawn for the surface area and the particle size; however, there seems to be some patterns for band gap (Fig. 3) even though they cannot be generalized because they are unique for the perovskite and the dopants.

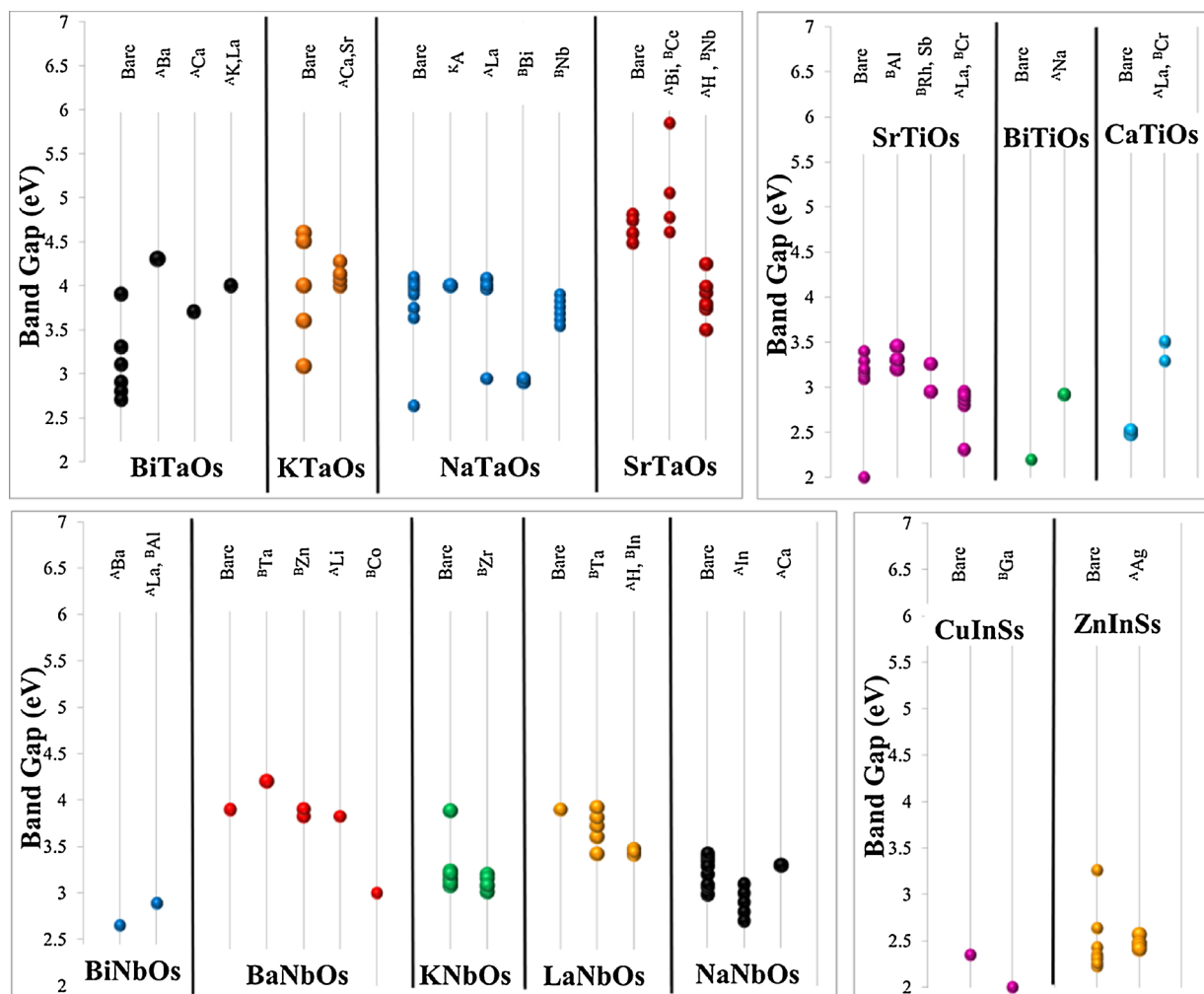


Fig. 3. Effects of doping on band gap of most commonly used perovskites.

3.3. Preparation methods for perovskites

The solid-state reaction (SSR) was the most common perovskite preparation method (188 cases in database); this followed by hydrothermal synthesis (HT) with 148 cases. Methods like polymerized-complex (PC), sol-gel (SG), ion-exchange (IE), electro-spinning (ES), Pechini-type process (PTP), flux-type and co-precipitation were also utilized. Fig. 4.a shows the frequency distribution of cases for the preparation methods together with the average hydrogen production. There are also novel and rarely used methods that are not included to Fig. (58 cases). Data for UV and visible light are presented separately; although the light source has no direct effects on catalyst preparation, it influences the method selection due to the band gap considerations.

Only HT and IE outperformed SSR in average hydrogen production; although the superiority of HT against SSR is known [32], having similar performance with SSR, SG and PC was surprising because the last two are also known to be better. For example, Jeong et al. reported that NiO/Sr₂Ti₂O₇ prepared by PC gave 1.33 times higher yield than SSR catalyst under UV due to its higher surface area and purity; PC method also prolonged the lifetime of catalyst [84]. Hu and Teng produced orthorhombic and cubic NaTaO₃ using SSR and SG respectively; SG-catalyst provided 23 times higher hydrogen production rates, and this was attributed to higher surface area, smaller particle size and high crystallinity due to lower calcination temperatures of SG (about 500 °C against 1200 °C for SSR) [85]. The results for NiO/InTaO₄ were also consistent with the results of previously mentioned article [86]; SG catalysts had smaller particle sizes, higher surface areas and enhanced

photocatalytic activities. These examples indicate that SG and PC methods are superior as long as they provide the desired physical properties described above, and apparently, this does not always happen as will be discussed later.

The HT method was also compared with SSR and PC in production of NaNbO₃ [32]. HT provided twice-higher yield than SSR while PC resulted in more than six times higher yield under UV if the calcination temperature was 600 °C; however, the yield was only 50% higher when the calcination temperature was 900 °C. The authors claimed that smaller catalyst size by PC (at 600 °C) may have shortened the diffusion distances of photogenerated electrons, and increased the number of electrons reached the active sites. Additionally, HT caused rectangular and cubic samples while SSR method resulted in spherical particles. The authors argued that the edges of HT catalysts may act as active sites. Hu et al. observed that UV activity of KTaO₃ prepared by SG was twice higher than that prepared by HT [87]. The higher surface area and advantageous crystalline structure of SG catalyst facilitated charge separation via more flattened Ta-O-Ta bond. New approaches were also tested and compared with conventional methods. For example, Liu et al. produced SrTiO₃ using PC, SSR and milling assistant method [32]; PC catalysts were the best due to their smaller size and uniformity of their components while the milling assistant method caused catalyst agglomeration and degradation. Similarly, Lee et al. synthesized SrSnO₃ by simple wet chemical reaction and compared the results with SSR; the catalysts obtained via the former method resulted in smaller particle size, better crystalline structure and five to ten times higher hydrogen production rate under UV [88].

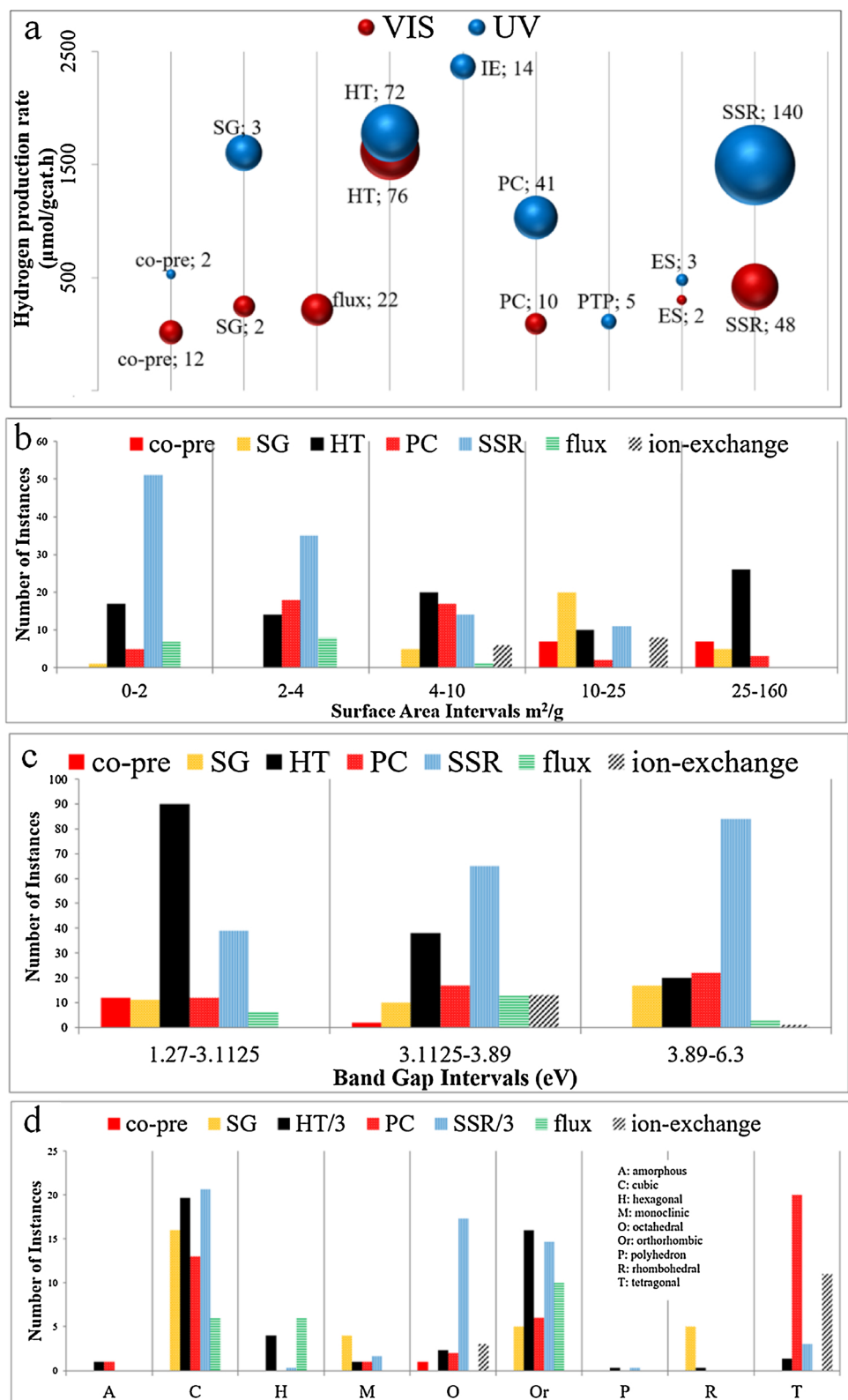


Fig. 4. Properties of perovskites prepared by the most commonly used perovskites average. a) hydrogen production rates b) surface area, c) band gap and d) crystal structure.

As clearly seen in Fig. 4.a, the average production rates are not in agreement with the examples above. HT delivered slightly higher average yield than SSR under UV while its visible light performances were much higher. Surprisingly the average UV and visible light performances of HT are also close to each other.

Researchers generally explain the effects of preparation methods through changes in particle size, surface area, crystal structure or band gap. Consequently, the dependence of those properties on the preparation methods was analyzed in more details. The surface area distributions with the most common methods are given in Fig. 4.b. (IE was

also added due to its high performance). SSR clearly produced surface areas in the lower side of distribution while SG did just the opposite; however, this difference did not seem to affect PWS activity. On the other hand, HT, which provides better hydrogen production rates, exhibits no clear trend in surface area. Only IE and PC exhibit some correlation between the surface area and performance; both surface area and hydrogen production rates are high for IE while both are relatively low for PC.

To analyze the effects of preparation method on bad gaps, the data were classified into three groups by this variable as 1.27–3.11 eV (700–400 nm) representing visible, 3.11–3.89 eV (400–320 nm) representing UV–A and 3.89–6.30 eV (320–290 nm) for UV–B & UV–C. The correlation between the band gap and preparation methods was undisputable for SSR and HT, (Fig. 4.c); SSR usually produces UV sensitive perovskites while HT resulted in lower band gaps explaining its higher visible light activity. The results are not conclusive for SG and PC while IE resulted in higher band gaps, which is in agreement with the fact that IE catalysts are tested under UV.

Fig. 4.d presents the crystal structures obtained by different methods. Both SSR and HT produce mostly orthorhombic and cubic structures while SSR also result in octahedral perovskites. To check the effect of this difference, the average performance of octahedral and the remaining SSR catalysts (orthorhombic and cubic) were compared. Indeed, the hydrogen production rate on octahedral structure (from 13 articles) was $866.5 \mu\text{mol gcat}^{-1} \text{h}^{-1}$ while it was $1079 \mu\text{mol gcat}^{-1} \text{h}^{-1}$ for remaining SSR data (orthorhombic and cubic from 38 articles). The crystal structure may also explain the results reported for PC perovskites. As Fig. 4.d shows, significant portion of PC perovskites are tetragonal although the remaining cases are cubic and orthorhombic as HT and SSR suggesting that the low average performance of PC may be due to tetragonal samples. Again, the average hydrogen production rate was found to be $256 \mu\text{mol gcat}^{-1} \text{h}^{-1}$ for tetragonal samples while it was $1650 \mu\text{mol gcat}^{-1} \text{h}^{-1}$ for the remaining data. However, it should be noted that the tetragonal samples are from the same source even though they contain various perovskites ($\text{Bi}_2\text{Ta}_2\text{O}_9$, $\text{Bi}_2\text{K}_{0.5}\text{La}_{0.5}\text{Ta}_2\text{O}_9$, $\text{Bi}_2\text{CaTa}_2\text{O}_9$ and $\text{Bi}_2\text{BaTa}_2\text{O}_9$) [45].

In summary, there are indeed correlations between the preparation methods and the perovskite properties like surface area, crystal structure and band gap. However, the direct impact of these properties on the average hydrogen production could not be established in this section; however, some patterns emerged in more detailed analyses in Section 4.

3.4. Co-catalyst for charge separation

One of the most effective ways to achieve charge separation in PWS is the use of co-catalysts; 424 instances out of 540 in the database were involved the use of a co-catalyst, which are usually transition metals and their oxides (Fig. 5) as it also stated in various reviews [89–92].

Pt is overwhelmingly the most common co-catalyst (178 data points), which was used with tantalates, niobates and titanates, and reported to improve hydrogen production [23]. However, Pt increased the hydrogen production up to a certain loading, and then it reduced photocatalytic activity due to shielding effect [45,64,93–95]; the optimal loading is depended on the perovskite. In general, Pt does not change morphological properties such as XRD pattern, surface area, pore characteristics and crystallite size [45,58,64,75,95]; it can slightly alter the band gap [34,58,32]. The photo deposition is the most common method (124 data points) for Pt loading; this is followed by impregnation (45 data points). Arney et al. compared these two methods and concluded that, while impregnation increased the activity by increasing surface area, the photo deposition contributed to the activity by smaller particle size and larger number of stepped surfaces [96]. In another work, the hydrogen production over the loaded (by photo deposition) and bare NaTaO_3 particles were analyzed, and it was noticed a delay in hydrogen production with the presence of Pt. It was

suggested that the photogenerated electrons were used for the Pt photo deposition first and then PWS starts [44]. The common result from all mentioned articles was that Pt enhanced the photocatalytic activity; it enabled charge separation, suppressed recombination, and provided active sites for hydrogen formation. However, the results in Fig. 5 do not support these results; average performance with Pt co-catalyst is lower than the average performance of bare semiconductors; apparently there are also low performance cases with Pt co-catalyst.

Rh was also used as co-catalyst. For example, Ham et al. impregnated Rh on SrTiO_3 and tested for PWS under visible light [71]; they proposed that Rh blocked the reverse reaction. Yoshida et al. studied Rh/ KTiO_3 under visible light, and found that different Rh loading was required for different preparation methods [97]. However, Takayama et al. studied several co-catalysts on $\text{KCaSrTa}_5\text{O}_{15}$, and they found that Rh was one of the less effective under UV [46]. As Pt, the average performance of Rh is also lower than the average obtained without a co-catalyst (Fig. 5).

Ru is a co-catalyst that was used with perovskite like SrTiO_3 , $\text{ZnIn}_{1.5}\text{S}_{3.2575}$, Ag:ZnInS , or $\text{KCaSrTa}_5\text{O}_{15}$ [38,46,70]; it was loaded by photo deposition in all those cases. Ru had the highest visible light activity in the database (Fig. 5); however, there are also works that showed its ineffectiveness. For example, Takayama et al. tested Rh, NiO, Ag, Au, and Pt as co-catalyst and Ru gave the minimum activity under UV [46].

Although there are only few cases in the database, Ag seems to be effective as co-catalyst. Shi and Guo photo deposited Ag over KTaO_3 and NaTaO_3 , and found that the behavior of Ag was very similar to Pt; it did not create changes in XRD pattern, particle size or surface area but broadened the light absorption capabilities. While hydrogen production rate was directly proportional to Ag loading until some point, the excessive loading lowered the catalytic activity [92]. There were also examples of Au, Cu, and Ni loading on several photocatalysts [34,46,98].

NiO_x is the most preferred co-catalyst among transition metal oxides (71 cases; second after Pt). It was used with several perovskites and worked particularly well with tantalates and niobates [33,45,67,82,88,89]. It has the highest average hydrogen production in the database (under UV). Since conduction band level of tantalates and niobates are generally higher than that of NiO_x , the photogenerated electrons in the conduction band of host perovskite can easily move to NiO_x providing charge separation [49,70,91,92]. Like Pt, NiO_x loading versus hydrogen production rate generally exhibited a volcanic shape; initial increase in rate is followed by a decline [1,2,25,46,68,70,99,100]. Li et al. explained this as the fact that the perovskite and NiO_x formed p-type and n-type semiconductors respectively; they had to be in optimum ratio to operate properly [82]. When NiO was loaded to tantalates, some Ni particles were reported to settle on the surface creating a core (Ni)-shell (NiO) structure providing selective diffusion of hydrogen and hydroxide ions. While hydrogen ion diffused to NiO and reduced, hydroxide could not; this prevents recombination of photogenerated oxygen and hydrogen [100]. In most cases, there was no obvious change in surface area, crystal size and absorption band with NiO_x loading [5,88,100].

RuO_x was also used due to its lower conduction band with respect to H^+/H energy level [101]; it works as electron trap to inhibit the recombination of photogenerated electron-hole pairs, facilitate oxygen production and suppress back reactions under visible light [25,68,102]. The activity generally increased with RuO_x loading first and reached a plateau; further increase of Ru loading gradually decreased the UV activity [25,68,103]. Torres-Martinez et al. had similar results with those of previously mentioned articles; they synthesized La:NaTaO_3 with SG method, which provided high surface area, and loaded with ruthenium oxide nanoparticles. High specific surface area enhanced RuO_2 dispersion and increased UV activity [103]. However, the surface area and crystal structure did not significantly changed by RuO_2 loading itself [32].

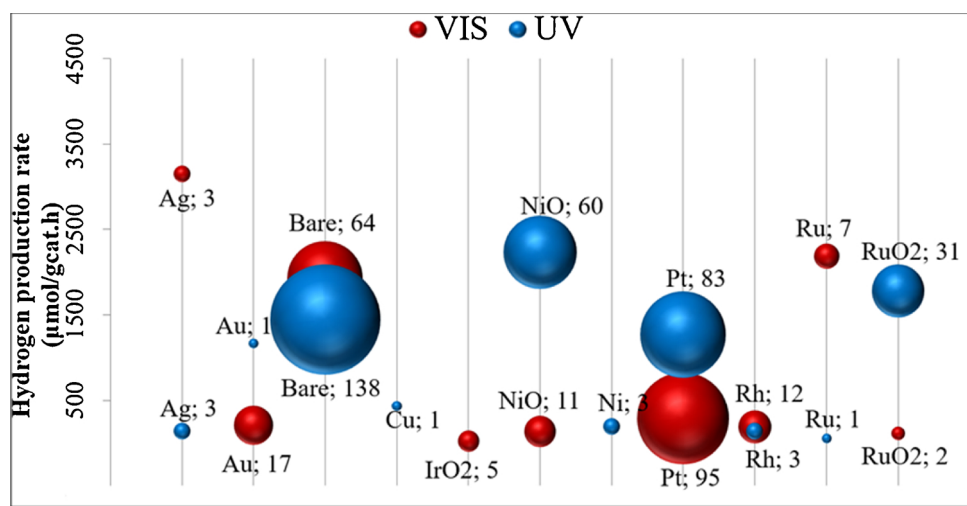


Fig. 5. Promoters used in the database vs. number of instances.

Although the co-catalyst loading differs depending on the co-catalyst itself and the perovskite used as semiconductor, there are some widely adopted ratios. For example, 1% Pt was used as co-catalyst in 48 cases out of 178 involving this metal while 45 cases had 0.5% Pt; the remaining cases utilized various Pt loading from 0.002% to 8%. This is also true for RuO₂; 17 of 33 cases used 1% RuO₂. On the other hand, there is no common loading level for NiO; various NiO loadings, from 0.022% to 5.02%, were used in 71 cases that have this oxide.

3.5. Thermal treatment

Calcination is a common thermal treatment that may affect morphological properties; it was applied in 351 data points (out of 540) in database. Various researchers showed that calcination temperature and time had a direct influence on particle size and surface area [32,36,71,79,84,85,104]. Generally, the particle size increases while the surface area decreases with increasing calcination temperature. The increase in particle size was attributed to the sintering [105]. Abe et al. found that La₃TaO₇ prepared by PC had a volcanic relation between its surface area and calcination temperature [36]. Crystallinity, purity, and sometimes band gap were also influenced by calcination temperature; usually, increasing calcination temperature increased the crystallinity and purity [36,84,85,104]. The crystallinity affected electrochemical conductivity and the mobility of photogenerated electron-hole pairs; the higher mobility implied higher probability of those pairs reaching to active sites [36]. Consequently, high calcination temperature may enhanced the activity through increasing crystallinity [32,36,79,105]. However, particle size, surface area, crystallinity, and band gap act on together; hence, there is an optimum combination of calcination temperature and time for high photocatalytic activity [79].

No clear patterns identified to link the calcination temperature to the surface area, particle size and crystal structure in database. However, the band gap seems to be correlated with calcination temperature; to see that, the band gap is divided into three classes (visible, UV-A and UV-B + UV-C) as in Section 3.3 (named as *visible*, *UV_A* and *UV_BC* in the following analyses) and the average calcination temperature of perovskites, which have the band gap in these intervals, were calculated based on the method used during their preparation. The band gaps of perovskite prepared by HT, PC and SG were increased with increasing average calcination temperature; there was no clear trend for SSR. For example, the average calcination temperatures were respectively 993.8 K, 1123 K, and 1225.3 K for *visible*, *UV_A* and *UV_BC* class perovskites prepared by PC method. The class division and results for other methods are presented in Supplementary Material.

3.6. Sacrificial agents and additives

Some chemicals were added to the reaction medium to improve hydrogen yield by acting as electron donors or acceptors and reducing back reaction of photogenerated electrons [23]. There are both organic and inorganic sacrificial agents; some are photodegradable while the others are not. Photodegradable industrial pollutants (like oxalic acid, formic acid and formaldehyde) are clearly more preferred to clean the environment while producing hydrogen [106]; however, if this is not intended, the sacrificial agent should be non-photodegradable for a long time.

3.6.1. Organic sacrificial agents

Methanol is the most common sacrificial agent (60% of data in database) [32,35,67,105,107,108]; there were also examples involving ethanol, propanol, formic acid and formaldehyde. Puangpetch et al. compared the performances of pure water, solution of methanol, ethanol, and propanol for PWS; methanol provided highest enhancement under UV [34]. The improvement was significant with 0–20 % methanol; then, it slowed down at higher percentages. Saadetnejad and Yildirim also verified this over Au/SrTiO₃; however, isopropyl alcohol was more effective if Al was doped on the catalyst [35].

Methanol degradation was also checked by previously mentioned articles, and found to be negligible [32,34,67,105,107,108]; this confirmed that methanol acted as hole scavenger and recombination blocker, but not hydrogen source [34]. There were also other articles verifying this result [32,67,101,102,55].

Methanol, propanol, formic acid, acetic acid, and formaldehyde were tested with SrTiO₃ under UV [31]; and the formic acid had the best performance. Stepwise reactions involving intermediates occurred with all sacrificial agents except formic acid; the competition between those intermediates with valence band holes inhibited hydrogen evolution. However, the reaction occurred in single step with formic acid promoting hydrogen evolution. The same group also found that average hydrogen production increases with formic acid concentration. There are also other works in which formaldehyde, formic acid, acetic acid and propanol were used as sacrificial agents indicating that the process could be also used to clean environment [80,81,100,104,109].

The data indicated that the alcohol (mostly methanol) concentration used with UV and visible light were quite similar; the ratio of the instances with 20% or below is 85% in visible data while it was 83% for UV.

3.6.2. Inorganic sacrificial agents

Inorganic compounds were also used as sacrificial agents, additives

to aqueous methanol solution, cut-off filters for light or to adjust pH of solution. Na_2S - Na_2SO_3 pair was commonly used due to their good hole scavenger performances [38,39,68,110,111]. NaNO_2 was also used frequently together with the other agents to cut-off UV light [37,49,68,112]. Xu et al. used NaOH to adjust the pH; the hydrogen evolution under visible light was the best in neutral solution [53]. Kato and Kudo utilized H_2SO_4 and NaOH to arrange pH; they obtained the maximum UV activity with NaOH (pH was 10.5) [113]. Lee et al. used KOH , NaOH , H_2SO_4 , CH_3COOH and Na_2SO_4 as sacrificial agents; the UV performance of CH_3COOH was much lower than the others [114]; the alkali solutions fastened the electron transfer between valence and conduction band [33]. There were also works in which AgNO_3 [115,34,44,71,73,84,33], FeCl_3 [44], KNO_3 [116], KOH [35], or NaI [58] were used.

As different from the organics, the inorganic additives were usually used for visible light experiments; while 37% of visible light instances in the database were obtained with inorganic additives, this number dropped to 8% for UV. Indeed, Na_2S - Na_2SO_3 , which was the most common choice, improved the average visible light activity from about 400 to 3000 $\mu\text{mol gcat}^{-1} \text{h}^{-1}$ while NaOH was effective under UV. The results for other common inorganic agents are given in Supplementary Material.

3.7. Light sources

The main purpose of PWS is to utilize the sunlight; hence, the use of UV light may not be rational because it constitutes only 4% of sunlight. However, most of the well-established photocatalysts (like TiO_2) work better under UV because of their high band gap. Although these materials are usually modified for visible light harvesting, they are also studied with UV as part of the efforts to understand PWS.

About 66% of data (324 data points) in the database were obtained under UV (mostly Hg lamb); the remaining 34% (158 data points) were generated under visible light (mostly Xe arc lamb). The average hydrogen production rate under UV was 1532.6 $\mu\text{mol gcat}^{-1} \text{h}^{-1}$ while it was 846.6 $\mu\text{mol gcat}^{-1} \text{h}^{-1}$ with visible light. Additionally, the hydrogen production rate was lower than 100 $\mu\text{mol gcat}^{-1} \text{h}^{-1}$ in 46% of instances for visible light whereas this ratio was only 28% for UV. The ratios of data with the rate higher than 1000 $\mu\text{mol gcat}^{-1} \text{h}^{-1}$ were 15% and 24% for visible and UV lights respectively.

3.8. Stability of perovskites

The stability of the perovskites used in PWS was also analyzed using the data from 53 papers reporting stability tests. Although, most of the factors discussed may affect the stability, only the effects of perovskites and dopants could be analyzed using available data. Even this could be done partially due to non-standard testing procedures; in these tests, the experiment is usually shut down after certain run time and re-started for a new run for the same time interval several times; the change of activity compared to the first run is used as the indicator of stability. Since the initial activity and duration of experiment changes from paper to paper, only the percent activity loss could be compared. Fig. 6 shows the results for tantalates; similar results for other perovskites are presented in Supplementary Material. Clearly, these results are not sufficient to deduce definitive conclusions; however, they provide some general idea for the effects of doping. For example, as two works at the bottom of Fig. 6 indicate, bare NaTaO_3 had significant loss in its stability after the first run, and Sr doping (third example from bottom) did not provide enhancement. However, La doping (fourth, fifth and sixth entries from bottom) improved the stability significantly (La and Cr co-doping even increased the performance in the second and third runs).

4. Analysis of database using data mining tools

4.1. Association rule mining for factor effects on hydrogen production

Association rule mining was used to determine the variables that may have significant effects on hydrogen production. The dataset (UV or visible) was divided into three performance classes (*low*, *medium* and *high* performance) as explained in Section 2. The analyses were restricted to the one-factor associations to determine simple and easy to follow deductions. Table 1 shows the top 10 factors (based on *lift* values) leading to high hydrogen production; the list of remaining important factors are presented in Supplementary Material.

The highest *lift* ratio (3) for *high* hydrogen production class for visible light belongs to ZnCdSs indicating that this is the most definitive way to have *high* hydrogen production rate. However, all 15 cases with ZnCdSs are already in *high* class; hence this factor is not suitable to appreciate the method; instead, a more complicated case, for which the data distributed among all three classes, would be more suitable. For example, the *support* of 0.13 (or 13%) for Na_2S as sacrificial agent indicates that the fraction of data *used Na_2S and resulted *high* hydrogen production* under visible light is 28, which is 13% of total visible data (28/216). There are total 72 data points with *high* hydrogen production; hence the *confidence* is 28/72 = 0.39; i.e. 39% of data having *high* hydrogen production rate involve Na_2S . If this ratio was also 39% in entire visible database, the use of Na_2S would not favor any class. However, there are 37 cases with Na_2S in entire data base; the ratio is 37/212 = 0.17, which is much lower than 0.39% for *high* class; then the *lift* is 0.39/0.17 = 2.27. This can be also stated as *fraction of data with Na_2S in *high* class is 2.29 times higher than the entire database*; this is a strong indicator for the benefit of Na_2S .

As the above example shows, higher *lift* indicates higher probability for intended result while higher *support* shows higher reliability because the number of data supporting this argument is large; we considered the results with the support higher than or equal to 0.05, which corresponds more than 11 and 16 data point for visible and UV datasets, for better generalization. Similar analysis can be also done for the other factors. However, the *novel preparation methods* (third in table) denote the collection of more than one method; hence, the rule should be interpreted as *the new approaches for catalyst preparation are somehow paid off*.

As can be seen from Table 1, the co-catalyst loading did not emerge as one of the most deterministic factor. There could be two possible explanations for this result. First, as Fig. 5 indicates, the presence of a co-catalyst does not seem to be an absolute necessity probably due to the properties of perovskites; some of them may have sites to accommodate both hydrogen and oxygen evolution themselves. The second reason is that the co-catalyst loading has been optimized to a certain value through years; for example it is a common practice to use about 0.5% or 1% Pt and 1% RuO_2 as discussed in Section 3.4. In other words, the variations in co-catalyst loadings in the database may not be sufficient to make significant changes in the performance and make this factor statistically significant.

The distribution of a data among three classes for a given alternative of a factor can be also determined using association rule mining; this can provide further evidences for the analysis performed in Section 3. For example, such an analysis for NaTaOs indicates that 63% of data containing these perovskites have *high* hydrogen production under visible light while this value is 30% and 7% for *medium* and *low* classes respectively. This clearly shows that NaTaOs are good choices for visible data. Similar results for the common factors are presented in are Supplementary Material.

4.2. Decision tree analysis to determine conditions for high hydrogen production

Decision tree classification (DT) was applied to UV and visible light

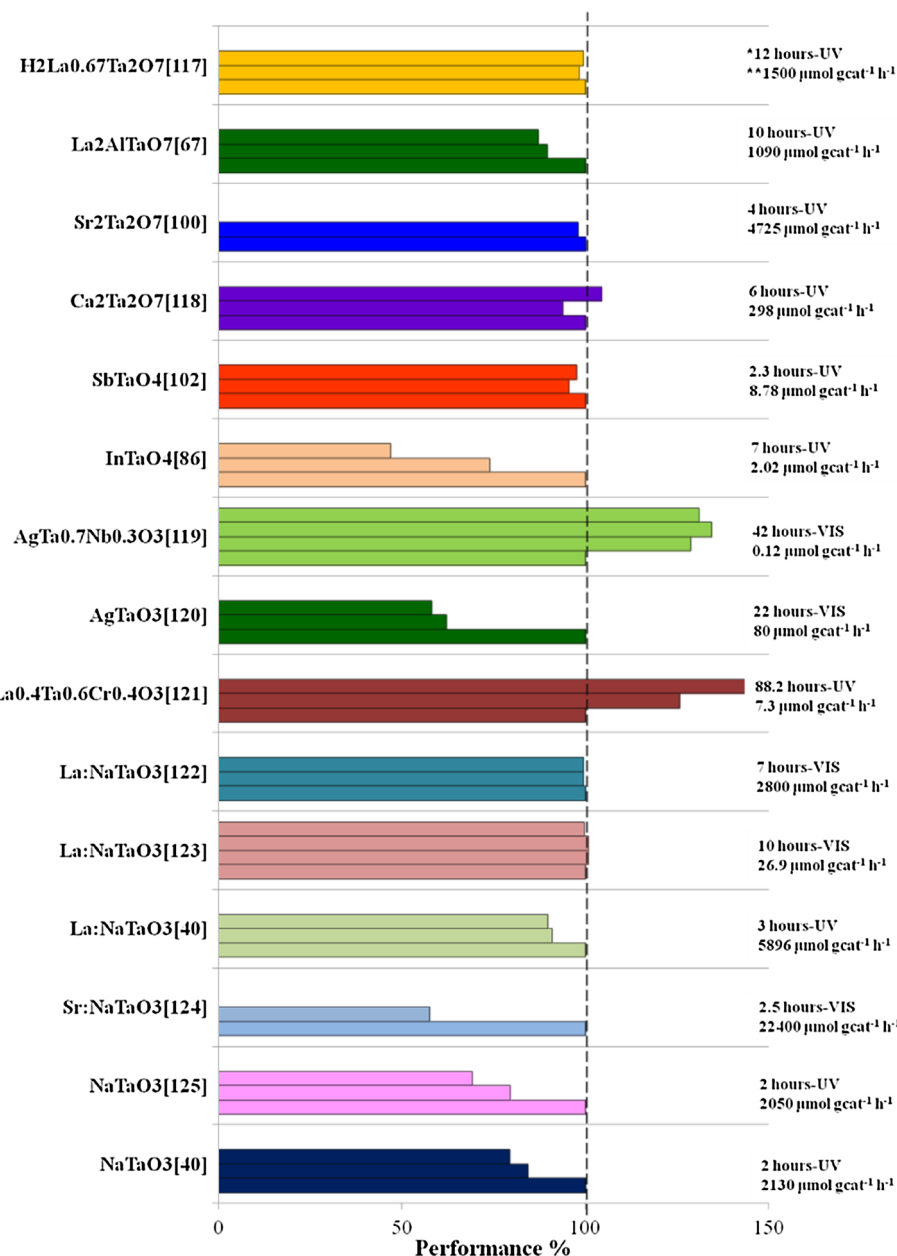


Fig. 6. Stability of some tantalates [40,67,86,100,102,117–125]. For each perovskite, bottom bar is the first run, the others are repeats in increasing order; *duration of test; **rate in first run.

data to develop potential guidelines and heuristics for future works. The model for visible light is summarized discussed below (Fig. 7). The classification accuracy was found to be 82%, which is quite high: the model correctly classified 82% of data (177 out of 216). The accuracy for *high*, *medium* and *low* classes were 76%, 82% and 88% respectively. More detailed information on accuracies as well as the model for UV are presented in Supplementary Material. As it will be apparent soon, the accuracy of individual branches is also important for rule deduction.

DT should be read from top to the terminal nodes through branches; the data satisfying condition stated in the node are sent to the left branch while the remaining data go to right. In Fig. 7, DT first divided the dataset by calcination time. Then the data with low calcination time were divided again by catalyst preparation method creating the leftmost terminal nodes containing 17% of data (37 out of 216) labeled as *high* with 86% accuracy; 32 of these 37 data indeed belong to *high* class (covers 44% of entire data in *high* class). This simple and statistically reliable result should be considered as a heuristic for the future studies.

Appearance of novel methods in the conditions leading high production rate was expected since a similar conclusion was also obtained with association rule mining above. Similarly, the calcination conditions are influential because they change the structure of the perovskite (note that order of appearance in the tree does not necessarily indicate the order of importance).

If SSR or novel methods were not used for perovskite preparation, the tree further divided the data by promoter suggesting that Au and Ag promoted catalyst would perform well. Then the divisions continued with A site elements and calcination conditions again.

On the right side, the tree divided the data by A-site of perovskite followed by crystal structure as it was also mentioned in Section 3, and reached the rightmost terminal node containing 24% data (52 out of 216), and labeled it as *low* performance with a remarkably high accuracy of 92% (48 of these 52 data belongs to *low* class). This is again a very strong sign that may be used as a heuristic for future studies.

Similar analysis can be performed for the branches leading to the

Table 1

Major factors leading high hydrogen production rate.

LHS Production rate level	RHS This feature was used in PWS belonging to production rate levels in LHS	Support This is fraction of all data belonging to class in LHS and has feature in RHS	Confidence This fraction of data in LHS has feature in RHS	Lift (This fraction of data in LHS has feature in RHS)/(this fraction of data in all data has feature in RHS)
VISIBLE 350 ($\mu\text{mol gcat}^{-1} \text{h}^{-1}$) and above	Undoped perovskite name = ZnCdS Preparation method = novel Sacrificial agent = $\text{Na}_2\text{S} + \text{Na}_2\text{SO}_3$ Surface Area = between 50 and 200 m^2/g Calcination time = 2 hours Undoped perovskite name = NaTaOs Promoter = no promoter Calcination time = no calcination Crystal = hexagonal Calcination temperature = no calcination	0.07 0.13 0.13 0.07 0.05 0.08 0.17 0.19 0.06 0.14	0.21 0.39 0.39 0.22 0.15 0.24 0.51 0.57 0.18 0.43	3.00 2.33 2.27 2.09 1.94 1.89 1.73 1.60 1.56 1.48
UV 550 ($\mu\text{mol gcat}^{-1} \text{h}^{-1}$) and above	Sacrificial Agent = NaNO_2 Alcohol% = between 10 and 20 % Surface area = between 10 and 15 m^2/g Undoped perovskite name = NaTaOs Calcination temperature = between 1400 and 1500 K Calcination time = no calcination Calcination temperature = no calcination Crystal structure = octahedral Calcination time = between 7 and 10 hours Calcination time = 2 hours	0.06 0.14 0.05 0.10 0.08 0.07 0.07 0.06 0.07	0.19 0.43 0.16 0.29 0.25 0.22 0.22 0.20 0.17 0.20	2.33 1.83 1.46 1.45 1.42 1.36 1.36 1.22 1.21 1.20

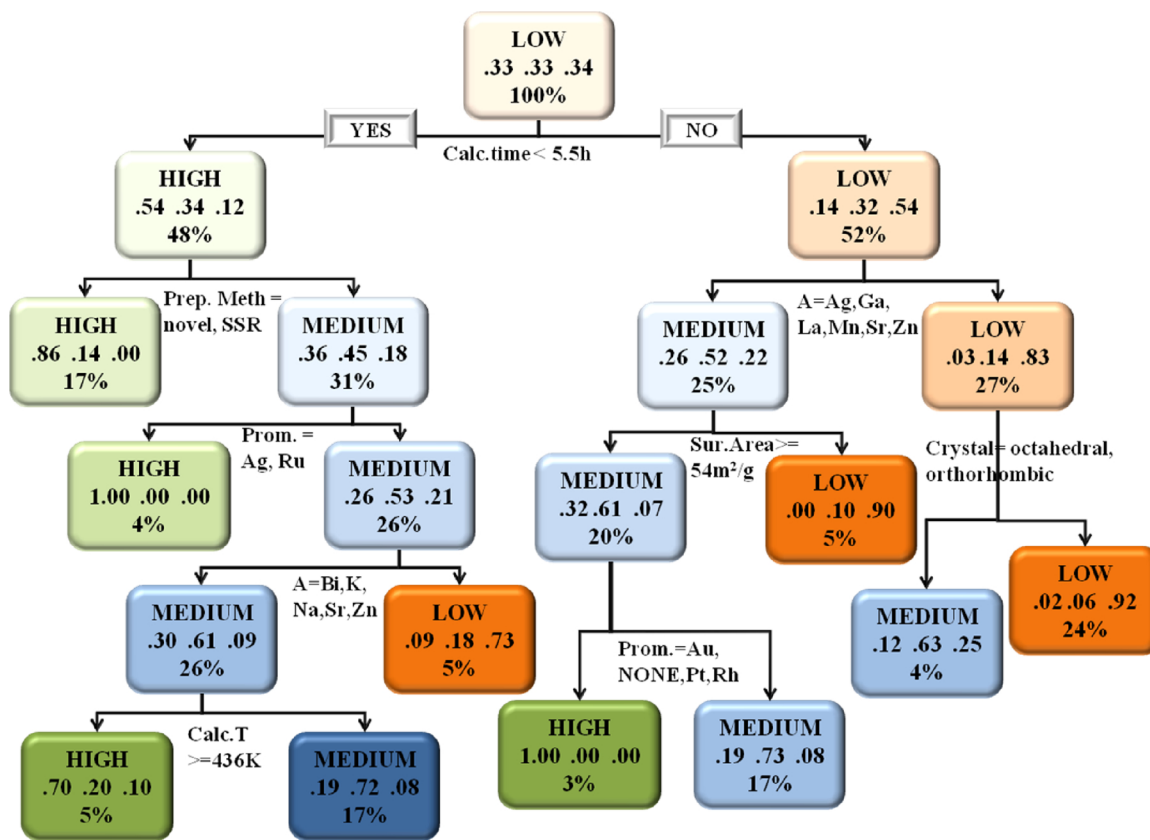


Fig. 7. The optimal decision tree for visible light data.

other terminal nodes with sufficiently large number of data points and accuracy. The branches that have such potential are also given in tabular form in Supplementary Material.

4.3. Random forest analysis to predict hydrogen production

Random forest (RF) regression was used to predict the hydrogen

production rate, and the predicted versus real rates for training and testing for visible light are presented in Fig. 8.a and 8.b respectively; each color in testing plot represents one set in 4-fold cross validation. The RMSE and R^2 for training were 558.1 and 0.95 for training. However, the true indicators for predictive power are RMSE (1194) and R^2 (0.79) for testing, in which the model is forced to predict the data not seen before; these values are quite high for a dataset constructed

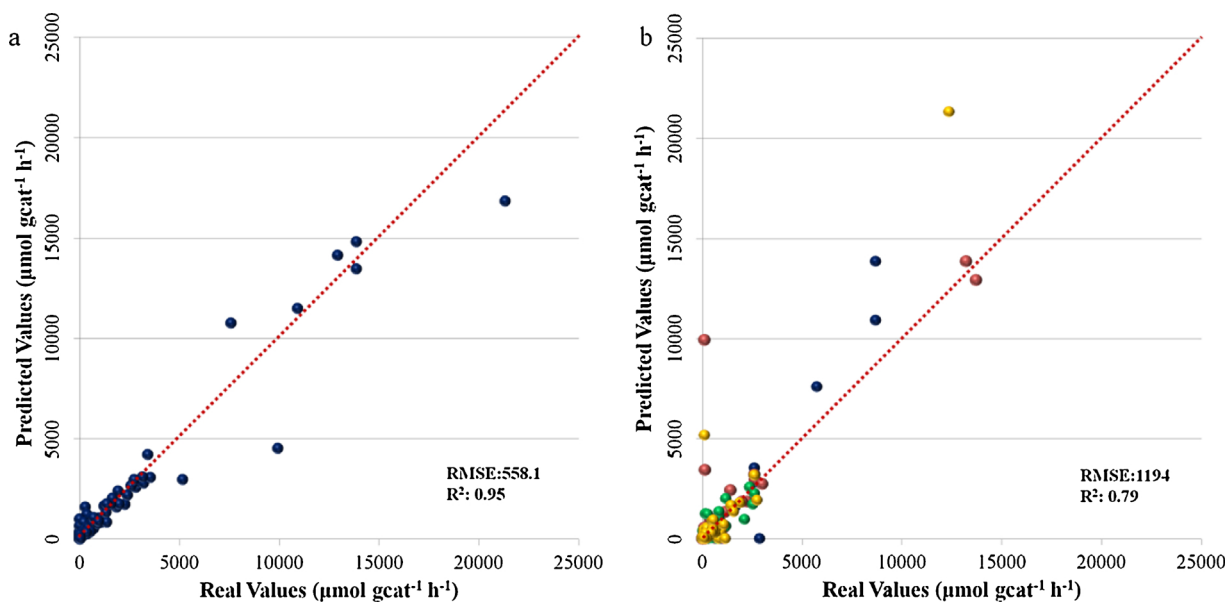


Fig. 8. Predicted versus actual hydrogen production for random forest model for visible light data a) training b) testing.

form 151 different sources. Although such a model may not be sufficient for high accuracy predictions, it can be used for initial assessments. The model for UV data was also given in Supplementary Material.

4.4. Analysis and modeling of band gaps

A new dataset (372 data points) was constructed from papers containing the band gaps of semiconductors as the output and the predictive variables affecting the material only; then it was analyzed using decision tree and random forest methods.

For decision tree analysis, the dataset was divided into three classes by band gaps as *visible*, *UV_A* and *UV_BC*. The further details are given in Supplementary Material while the optimum tree found is in Fig. 9a. The classification accuracy was 78%, which is quite good, while it was 89%, 56% and 75% for *low*, *medium* and *high* classes respectively.

The data was first divided by B-site of perovskite, and then the left branch was divided by A-side reaching to the leftmost terminal node containing 20% of the data (48% of visible light data). Both the number of data and the purity of the node (92%) are remarkably high so that this branch can be used as a heuristic for material selection. After the first division in the left, the model used B-side doping, and generates the second leftmost terminal node with 100% purity covering 5% of the data; the rule described in this branch can be also safely used for the future works.

On the right, the tree proceeds with further refinement with B-side doping (with type and then loading). The first division separated the *visible* region from the others while the second divided *UV_A* and *UV_BC*. The purity (79%) and the reliability (30% of data, 77% of *UV_BC* data) of the rightmost node is also significantly high.

As it clearly seen from the branches involving both visible and UV classes, the doping seems to be the most dominant factor (the tree utilizes B site doping more than A site for discrimination). This is in complete agreement with the literature that the main objective of doping is usually changing the band gap. However, the band gap modification, unfortunately, not always make the desirable improvement in the hydrogen production as it is evident from the review presented in Section 3 and decision tree in Section 4.3 (doping was not the most important factor for hydrogen production).

Random forest regression was used to predict the band gap from input variables; the predicted versus real band gap plots for the optimal model are presented in Fig. 9b and c for training and testing

respectively (colors characterizes subsets in cross validation). The RMSE and R^2 values for training were 0.24 and 0.94 respectively while the average results for the testing were 0.51 for RMSE and 0.61 for R^2 . Even though model may not be sufficient for precise predictions, it has some prediction ability, which can be further improved with the addition of new data, and used for initial assessment in band gap modifications [126–129].

Models correlating the band gap and the hydrogen production rate were also tested but the model fitness was not sufficiently high. This also verifies the conclusion from Section 3, and decision tree analyses above, that the relation between the band gap and the hydrogen production rate is not always straightforward.

5. Conclusion

The aim of this work was to analyze the past publications on PWS over perovskites using data mining tools to assess the present status, identify the major trends and patterns in past works and draw the conclusions for the future studies. The conclusion can be summarized as follows:

- The most common perovskites in PWS are tantalates followed by titanates, niobates and In-perovskites. NaTaOs are the most frequently studied tantalates, and they are especially effective under UV light. The most common titanates are SrTiOs, which are also better under UV but they are mostly tested under visible light.
- About half (48%) of perovskites in database are doped to A-site (31%) and/or B-site (27%). The effect of doping on band gap is observable; however, only some portion of doped catalysts had better PWS activity than plain perovskites. The doping also improved stability in some cases.
- Solid-state reaction, hydrothermal synthesis, polymerized-complex and sol-gel are the most common methods for perovskite preparation; their average performances are similar for UV tests despite the reports claiming the limitations of solid-state reaction. However, hydrothermal synthesis clearly performs better in average under the visible light. Effects of preparation method on surface area, band gap and crystal structure are also observable; the last two partially explain the hydrogen production rates as well.
- Approximately 80% of cases contain co-catalyst (Pt is the most common). There are various successful applications; however, in overall, only some fraction of co-catalyst results in higher

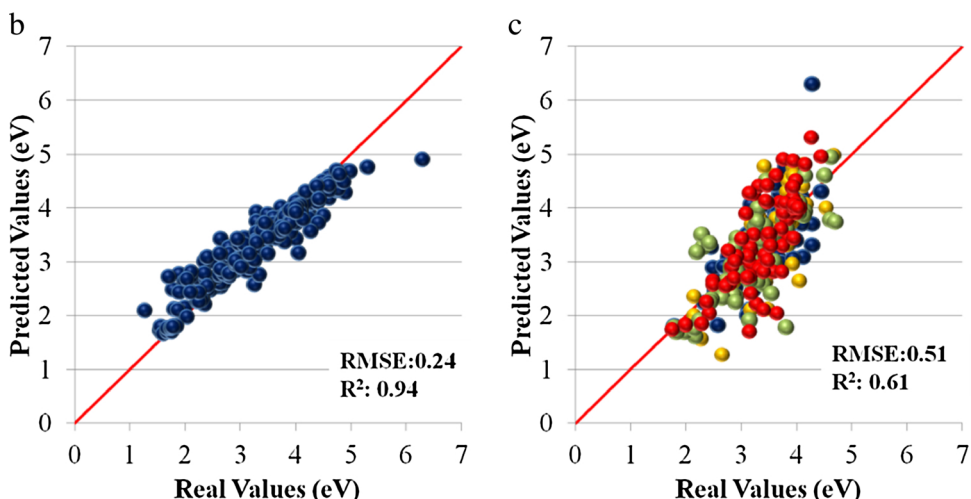
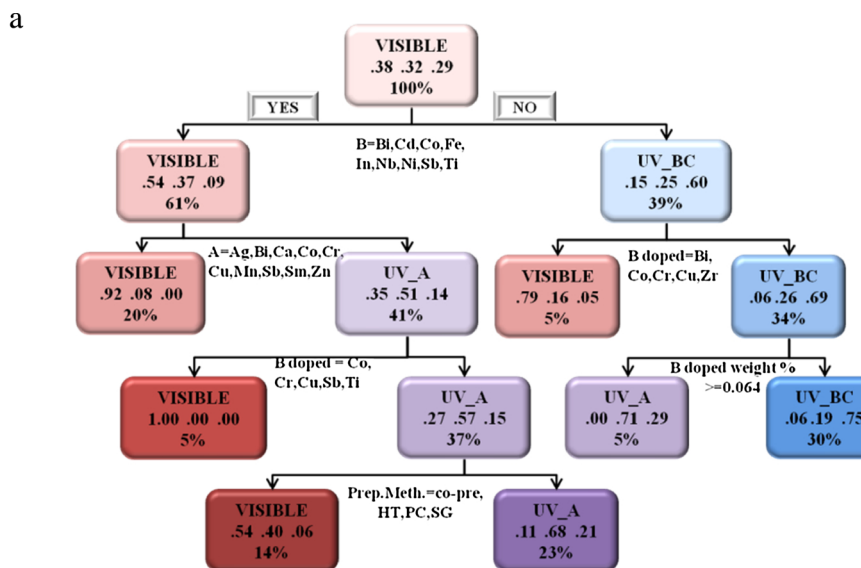


Fig. 9. Results of the analysis of band gaps a) decision tree constructed for band gaps b) training results of random forest analysis c) testing results of random forest analysis.

performance than the bare perovskites.

- The methanol (20% or less) is used as sacrificial agent in about 80% of the tests (both UV and visible light), and found to be beneficial; some other organic sacrificial agents are also used. The inorganics additives, on the other hand, are usually used in visible light tests.
- Association rule mining clearly identifies the most influential factors for high hydrogen production, and verifies the conclusions obtained from the review of literature. However, no single factor dominates the result; large number of factors affect the performance.
- Decision tree analysis provides some simple and easy to follow selection rules and heuristics for both hydrogen production and band gap. The selection rules seems to be clearer for the band gap; the doping (especially in B site) is the most determining factor for the band gap as intended.
- Random forest models for hydrogen production (especially for visible light) are quite successful in predicting the data not seen before; hence, they can be used for initial estimates even though they are not sufficient for the high accuracy predictions. The same is true for band gap prediction; the random forest model for the band gap prediction is also very successful. However, a model directly correlating the band gap with the hydrogen production rate could not be established.

Considering the clear trends in analyses and the high fitness of the models constructed using the data from 151 different sources, it can be concluded that PWS over perovskites is predictable. However, non-standard testing procedure makes the generalization harder (especially for stability).

It is hard to identify few significant factors that may be fine-tuned and improve PWS; many factors seem to be effective, and the improvement obtained is always limited. The sound solutions like ion doping to change band gap, use of co-catalyst for change separation or use of additives as sacrificial agents definitely help to improve the results but not as much as it is desired; there seems to be a need for new approaches.

Appendix A. Supplementary data

Supplementary material related to this article can be found, in the online version, at doi:<https://doi.org/10.1016/j.apcatb.2018.09.104>.

References

- [1] R. Kothari, D. Buddhi, R.L. Sawhney, Comparison of environmental and economic aspects of various hydrogen production methods, *Renew. Sust. Energy Rev.* 12

(2008) 553–563, <https://doi.org/10.1016/j.rser.2006.07.012>.

[2] I. Dincer, C. Acar, Review and evaluation of hydrogen production methods for better sustainability, *Int. J. Hydrogen Energy* 40 (2014) 11094–11111, <https://doi.org/10.1016/j.ijhydene.2014.12.035>.

[3] A. Fujishima, K. Honda, Electrochemical photolysis of water at a semiconductor electrode, *Nature* 238 (1972) 37–38, <https://doi.org/10.1038/238037a0>.

[4] Y. Ma, X. Wang, Y. Jia, X. Chen, H. Han, C. Li, Titanium dioxide-based nanomaterials for photocatalytic fuel generations, *Chem. Rev.* 114 (2014) 9987–10043, <https://doi.org/10.1021/cr500008u>.

[5] J. Li, N. Wu, Semiconductor-based photocatalysts and photoelectrochemical cells for solar fuel generation: a review, *Catal. Sci. Technol.* 5 (2015) 1360–1384, <https://doi.org/10.1039/c4cy00974f>.

[6] M. Ge, J. Cai, J. Iocozzia, C. Cao, J. Huang, X. Zhang, J. Shen, S. Wang, S. Zhang, K.Q. Zhang, Y. Lai, Z. Lin, A review of TiO_2 nanostructured catalysts for sustainable H_2 generation, *Int. J. Hydrogen Energy* 42 (2017) 8418–8449, <https://doi.org/10.1016/j.ijhydene.2016.12.052>.

[7] K. Emery, Reference Solar Spectral Irradiance Air Mass 1.5, (2018) (accessed 01 August 2018), <http://rredc.nrel.gov/solar/spectra/am1.5/>.

[8] S. Fukuzumi, D. Hong, Y. Yamada, Bioinspired photocatalytic water reduction and oxidation with earth-abundant metal catalysts, *J. Phys. Chem. Lett.* 4 (2013) 3458–3467, <https://doi.org/10.1021/jz401560x>.

[9] M.E. Günay, R. Yıldırım, Knowledge extraction from catalysis of the past: a case of selective CO oxidation over noble metal catalysts between 2000 and 2012, *ChemCatChem.* 5 (2013) 1395–1406, <https://doi.org/10.1002/cctc.201200665>.

[10] Ç. Odabaşı, M.E. Günay, R. Yıldırım, Knowledge extraction for water gas shift reaction over noble metal catalysts from publications in the literature between 2002 and 2012, *Int. J. Hydrogen Energy* 39 (2014) 5733–5746, <https://doi.org/10.1016/j.ijhydene.2014.01.160>.

[11] M. Baysal, M.E. Günay, R. Yıldırım, Decision tree analysis of past publications on catalytic steam reforming to develop heuristics for high performance: a statistical review, *Int. J. Hydrogen Energy* 42 (2017) 243–254, <https://doi.org/10.1016/j.ijhydene.2016.10.003>.

[12] A.N. Şener, M.E. Günay, A. Leba, R. Yıldırım, Statistical review of dry reforming of methane literature using decision tree and artificial neural network analysis, *Catal. Today* 299 (2018) 289–302, <https://doi.org/10.1016/j.cattod.2017.05.012>.

[13] N.A. Tapan, M.E. Günay, R. Yıldırım, Constructing global models from past publications to improve design and operating conditions for direct alcohol fuel cells, *Chem. Eng. Res. Des.* 105 (2016) 162–170, <https://doi.org/10.1016/j.cherd.2015.11.018>.

[14] D. Chesterfield, A.A. Adesina, Evidence-based design and optimisation of titania photocatalysts via artificial neural network analysis, *J. Chem. Eng. Jpn.* 42 (2009) 185–198, <https://doi.org/10.1252/jcej.08we210>.

[15] E.V. Kondratenko, M. Schlüter, M. Baerns, D. Linke, M. Holena, Developing catalytic materials for the oxidative coupling of methane through statistical analysis of literature data, *Catal. Sci. Technol.* 5 (2015) 1668–1677, <https://doi.org/10.1039/C4CY01443J>.

[16] T. Davran-Candan, M.E. Günay, Structure and activity relationship for CO and O_2 adsorption over gold nanoparticles using density functional theory and artificial neural networks, *J. Chem. Phys.* 132 (2010) 174113, <https://doi.org/10.1063/1.3369007>.

[17] A.A. Emery, J.E. Saal, S. Kirklin, V.I. Hegde, C. Wolverton, High-throughput computational screening of perovskites for thermochemical water splitting applications, *Chem. Mater.* 28 (2016) 5621–5634, <https://doi.org/10.1021/acs.chemmater.6b01182>.

[18] J. Graser, S.K. Kauwe, T.D. Sparks, Machine learning and energy minimization approaches for crystal structure predictions: a review and new horizons, *Chem. Mater.* 30 (2018), <https://doi.org/10.1021/acs.chemmater.7b05304>.

[19] M. Hahsler, C. Buchta, B. Gruen, A. Michael, C. Buchta, B. Gruen, K. Hornik, I. Johnson, Package ‘Arules’, (2018).

[20] T. Therneau, B. Atkinson, B. Ripley, Package ‘rpart’, (2018), p. 34.

[21] A. Liaw, M. Wiener, Package ‘randomForest’, (2018).

[22] A.A. Ismail, D.W. Bahnamann, Photochemical splitting of water for hydrogen production by photocatalysis: A review, *Sol. Energy Mater. Sol. Cells* 128 (2014) 85–101, <https://doi.org/10.1016/j.solmat.2014.04.037>.

[23] X. Chen, S. Shen, L. Guo, S.S. Mao, Semiconductor-based photocatalytic hydrogen generation, *Chem. Rev.* 110 (2010) 6503–6570, <https://doi.org/10.1021/cr1001645>.

[24] J.W. Liu, G. Chen, Z.H. Li, Z.G. Zhang, Hydrothermal synthesis and photocatalytic properties of $AlTaO_3$ and $AlNbO_3$ ($A = Na$ and K), *Int. J. Hydrogen Energy* 32 (2007) 2269–2272, <https://doi.org/10.1016/j.ijhydene.2006.10.005>.

[25] C. Gómez-Solís, M.A. Ruiz-Gómez, L.M. Torres-Martínez, I. Juárez-Ramírez, D. Sánchez-Martínez, Facile solvo-combustion synthesis of crystalline $NaTaO_3$ and its photocatalytic performance for hydrogen production, *Fuel* 130 (2014) 221–227, <https://doi.org/10.1016/j.fuel.2014.04.019>.

[26] Y. Li, G. Chen, H. Zhang, Z. Li, J. Sun, Electronic structure and photocatalytic properties of $AlBi_2Ta_2O_9$ ($A = Ca, Sr, Ba$), *J. Solid State Chem.* 181 (2008) 2653–2659, <https://doi.org/10.1016/j.jssc.2008.05.020>.

[27] T.N. Obee, R.T. Brown, TiO_2 photocatalysis for Indoor Air Applications: Effects of Humidity and Trace Contaminant Levels on the Oxidation Rates of Formaldehyde, Toluene, and 1,3-Butadiene, *Environ. Sci. Technol.* 29 (1995) 1223–1231, <https://doi.org/10.1021/es00050a013>.

[28] P. Nikolaidis, A. Poulikkas, A comparative overview of hydrogen production processes, *Renew. Sust. Energy Rev.* 67 (2017) 597–611, <https://doi.org/10.1016/j.rser.2016.09.044>.

[29] A. Iwase, H. Kato, A. Kudo, The effect of alkaline earth metal ion dopants on photocatalytic water splitting by $NaTaO_3$ powder, *ChemSusChem* 2 (2009) 873–877, <https://doi.org/10.1002/cssc.200900160>.

[30] B. Zielińska, E. Borowiak-Palen, R.J. Kalenczuk, Photocatalytic hydrogen generation over alkaline-earth titanates in the presence of electron donors, *Int. J. Hydrogen Energy* 33 (2008) 1797–1802, <https://doi.org/10.1016/j.ijhydene.2008.02.001>.

[31] C.C. Hu, H. Teng, Structural features of p-type semiconducting NiO as a co-catalyst for photocatalytic water splitting, *J. Catal.* 272 (2010) 1–8, <https://doi.org/10.1016/j.jcat.2010.03.020>.

[32] G. Li, T. Kako, D. Wang, Z. Zou, J. Ye, Synthesis and enhanced photocatalytic activity of $NaNbO_3$ prepared by hydrothermal and polymerized complex methods, *J. Phys. Chem. Solids* 69 (2008) 2487–2491, <https://doi.org/10.1016/j.jpcs.2008.05.001>.

[33] Y. Liu, L. Xie, Y. Li, R. Yang, J. Qu, Y. Li, X. Li, Synthesis and high photocatalytic hydrogen production of $SrTiO_3$ nanoparticles from water splitting under UV irradiation, *J. Power Sources* 183 (2008) 701–707, <https://doi.org/10.1016/j.jpowsour.2008.05.057>.

[34] T. Puangpetch, T. Sreethawong, S. Chavadej, Hydrogen production over metal-loaded mesoporous-assembled $SrTiO_3$ nanocrystal photocatalysts: Effects of metal type and loading, *Int. J. Hydrogen Energy* 35 (2010) 6531–6540, <https://doi.org/10.1016/j.ijhydene.2010.04.015>.

[35] D. Saadetnejad, R. Yıldırım, Photocatalytic hydrogen production by water splitting over $Al-AlSrTiO_3$, *Int. J. Hydrogen Energy* 43 (2018) 1116–1122, <https://doi.org/10.1016/j.ijhydene.2017.10.154>.

[36] R. Abe, M. Higashi, K. Sayama, Y. Abe, H. Sugihara, Photocatalytic Activity of R_3MO_7 and $R_2Ti_2O_7$ ($R = Y, Gd, La; M = Nb, Ta$) for Water Splitting into H_2 and O_2 , *J. Phys. Chem. B* 110 (2006) 2219–2226, <https://doi.org/10.1021/jp0552933>.

[37] B. Naik, S. Martha, K.M. Parida, Facile fabrication of $Bi_2O_3/TiO_{2-x}N_x$ nanocomposites for excellent visible light driven photocatalytic hydrogen evolution, *Int. J. Hydrogen Energy* 36 (2011) 2794–2802, <https://doi.org/10.1016/j.ijhydene.2010.11.104>.

[38] F. Li, J. Luo, G. Chen, Y. Fan, Q. Huang, Y. Luo, D. Li, Q. Meng, Hydrothermal synthesis of zinc indium sulfide microspheres with Ag^+ doping for enhanced H_2 production by photocatalytic water splitting under visible light, *Catal. Sci. Technol.* 4 (2014) 1144–1150, <https://doi.org/10.1039/C3CY00952A>.

[39] K. Song, R. Zhu, F. Tian, G. Cao, F. Ouyang, Effects of indium contents on photocatalytic performance of $ZnIn_2S_4$ for hydrogen evolution under visible light, *J. Solid State Chem.* 232 (2015) 138–143, <https://doi.org/10.1016/j.jssc.2015.09.025>.

[40] A. Kudo, H. Kato, Effect of lanthanide-doping into $NaTaO_3$ photocatalysts for efficient water splitting, *Chem. Phys. Lett.* 331 (2000) 373–377, [https://doi.org/10.1016/S0009-2614\(00\)01220-3](https://doi.org/10.1016/S0009-2614(00)01220-3).

[41] H. Kato, K. Asakura, A. Kudo, Highly efficient water splitting into H_2 and O_2 over lanthanum-doped $NaTaO_3$ photocatalysts with high crystallinity and surface nanostructure, *J. Am. Chem. Soc.* 125 (2003) 3082–3089, <https://doi.org/10.1021/ja027751g>.

[42] H. Husin, Y.S. Adisalamun, T.M. Asnawi, F. Hasfita, Pt nanoparticle on $La_{0.02}Na_{0.98}TaO_3$ catalyst for hydrogen evolution from glycerol aqueous solution, *AIP Conf. Proc.* 1788 (2017) 0–6, <https://doi.org/10.1063/1.4968326>.

[43] H. Husin, H.M. Chen, W.N. Su, C.J. Pan, W.T. Chuang, H.S. Sheu, B.J. Hwang, Green fabrication of La-doped $NaTaO_3$ via H_2O_2 assisted sol-gel route for photocatalytic hydrogen production, *Appl. Catal. B Environ.* 102 (2011) 343–351, <https://doi.org/10.1016/j.apcatb.2010.12.024>.

[44] P. Jana, C. Mata Montero, P. Pizarro, J.M. Coronado, D.P. Serrano, V.A. De La Peña O’Shea, Photocatalytic hydrogen production in the water/methanol system using $Pt/RE:NaTaO_3$ ($RE = Y, La, Ce, Yb$) catalysts, *Int. J. Hydrogen Energy* 39 (2014) 5283–5290, <https://doi.org/10.1016/j.ijhydene.2013.12.182>.

[45] W. Chen, X. Chen, Y. Yang, J. Yuan, W. Shangguan, Synthesis and performance of layered perovskite-type $H-Abi_2Ta_2O_9$ ($A = Ca, Sr, Ba, K_{0.5}La_{0.5}$) for photocatalytic water splitting, *Int. J. Hydrogen Energy* 39 (2014) 13468–13473, <https://doi.org/10.1016/j.ijhydene.2014.03.096>.

[46] T. Takayama, K. Tanabe, K. Saito, A. Iwase, A. Kudo, The $KCaSrTa_5O_{15}$ photocatalyst with tungsten bronze structure for water splitting and CO_2 reduction, *Phys. Chem. Chem. Phys.* 16 (2014) 24417–24422, <https://doi.org/10.1039/C4CP03892D>.

[47] W. Chen, C. Li, H. Gao, J. Yuan, W. Shangguan, J. Su, Y. Sun, Photocatalytic water splitting on protonated form of layered perovskites $K_{0.5}La_{0.5}Bi_2M_2O_9$ ($M = Ta; Nb$) by ion-exchange, *Int. J. Hydrogen Energy* 37 (2012) 12846–12851, <https://doi.org/10.1016/j.ijhydene.2012.05.090>.

[48] K.I. Shimizu, S. Itoh, T. Hatamachi, T. Kodama, M. Sato, K. Toda, Photocatalytic water splitting on ni-intercalated ruddlesden-popper tantalate $H_2La_{2/3}Ta_2O_7$, *Chem. Mater.* 17 (2005) 5161–5166, <https://doi.org/10.1021/cm050982c>.

[49] Y. Huang, Y. Li, Y. Wei, M. Huang, J. Wu, Photocatalytic property of partially substituted Pt-intercalated layered perovskite, $ASr_2Ta_4Nb_{3-x}O_{10}$ ($A = K, H; X = 0, 1, 1.5, 2$ and 3), *Sol. Energy Mater. Sol. Cells* 95 (2011) 1019–1027, <https://doi.org/10.1016/j.solmat.2010.12.017>.

[50] T. Ishii, H. Kato, A. Kudo, H_2 evolution from an aqueous methanol solution on $SiTiO_3$ photocatalysts codoped with chromium and tantalum ions under visible light irradiation, *J. Photochem. Photobiol. A: Chem.* 163 (2004) 181–186.

[51] F. Cai, Y. Meng, B. Hu, Y. Tang, W. Shi, Microwave-assisted synthesis of La–Cr co-doped $SiTiO_3$ nano-particles and their use in photocatalytic hydrogen evolution under visible light, *RSC Adv.* 5 (2015) 57354–57360, <https://doi.org/10.1039/C5RA04659A>.

[52] W. Luo, Z. Li, X. Jiang, T. Yu, L. Liu, X. Chen, J. Ye, Z. Zou, Correlation between the band positions of $(SrTiO_3)_{1-x}(LaTiO_2N)_x$ solid solutions and photocatalytic properties under visible light irradiation, *Phys. Chem. Chem. Phys.* 10 (2008)

6717, <https://doi.org/10.1039/b803996h>.

[53] L. Lu, S. Ni, G. Liu, X. Xu, Structural dependence of photocatalytic hydrogen production over La/Cr co-doped perovskite compound ATiO_3 (A = Ca, Sr and Ba), *Int. J. Hydrogen Energy* 42 (2017) 23539–23547, <https://doi.org/10.1016/j.ijhydene.2017.01.064>.

[54] D. Wang, J. Ye, T. Kako, T. Kimura, Photophysical and Photocatalytic Properties of SrTiO_3 Doped with Cr Cations on Different Sites, *J. Phys. Chem. B* 110 (2006) 15824–15830.

[55] T. Takata, K. Domen, Defect engineering of photocatalysts by doping of aliovalent metal cations for efficient water splitting, *J. Phys. Chem. C* 113 (2009) 19386–19388, <https://doi.org/10.1021/jp908621e>.

[56] Q. Li, T. Kako, J. Ye, Facile ion-exchanged synthesis of Sn^{2+} incorporated potassium titanate nanoribbons and their visible-light-responded photocatalytic activity, *Int. J. Hydrogen Energy* 36 (2011) 4716–4723, <https://doi.org/10.1016/j.ijhydene.2011.01.082>.

[57] J. Shi, J. Ye, Z. Zhou, M. Li, L. Guo, Hydrothermal synthesis of $\text{Na}_{0.5}\text{La}_{0.5}\text{TiO}_3\text{-LaCrO}_3$ solid-solution single-crystal nanocubes for visible-light-driven photocatalytic H_2 evolution, *Chem. - A Eur. J.* 17 (2011) 7858–7867, <https://doi.org/10.1002/chem.201003755>.

[58] Y. Li, J. Wu, Y. Huang, M. Huang, J. Lin, Photocatalytic water splitting on new layered perovskite $\text{A}_{2.33}\text{Sr}_{0.67}\text{Nb}_5\text{O}_{14.335}$ (A = K, H), *Int. J. Hydrogen Energy* 34 (2009) 7927–7933, <https://doi.org/10.1016/j.ijhydene.2009.07.047>.

[59] Y. Wei, J. Li, Y. Huang, M. Huang, J. Lin, J. Wu, Photocatalytic water splitting with In-doped $\text{H}_2\text{LaNb}_2\text{O}_7$ composite oxide semiconductors, *Sol. Energy Mater. Sol. Cells* 93 (2009) 1176–1181, <https://doi.org/10.1016/j.solmat.2009.02.001>.

[60] J. Yin, Z. Zou, J. Ye, A novel series of the new visible-light-driven photocatalysts $\text{MCo}_{1/3}\text{Nb}_{2/3}\text{O}_3$ (M = Ca, Sr, and Ba) with special electronic structures, *J. Phys. Chem. B* 107 (2003) 4936–4941, <https://doi.org/10.1021/JP0340919>.

[61] J. Yin, Z. Zou, J. Ye, Photophysical and Photocatalytic Properties of $\text{MIn}_{0.5}\text{Nb}_{0.5}\text{O}_3$ (M = Ca, Sr, and Ba), *J. Phys. Chem. B* 107 (2003) 61–65, <https://doi.org/10.1021/jp026403y>.

[62] Y. Li, G. Chen, H. Zhang, Z. Lv, Band structure and photocatalytic activities for H_2 production of $\text{ABi}_2\text{Nb}_2\text{O}_9$ (A = Ca, Sr, Ba), *Int. J. Hydrogen Energy* 35 (2010) 2652–2656, <https://doi.org/10.1016/j.ijhydene.2009.04.021>.

[63] H.W. Kang, S.N. Lim, S. Bin Park, Photocatalytic H_2 evolution under visible light from aqueous methanol solution on $\text{NaBi}_x\text{Ta}_{1-x}\text{O}_3$ prepared by spray pyrolysis, *Int. J. Hydrogen Energy* 37 (2012) 4026–4035, <https://doi.org/10.1016/j.ijhydene.2011.12.006>.

[64] P. Kanhere, J. Zheng, Z. Chen, Visible light driven photocatalytic hydrogen evolution and photophysical properties of Bi^{3+} doped NaTaO_3 , *Int. J. Hydrogen Energy* 37 (2012) 4889–4896, <https://doi.org/10.1016/j.ijhydene.2011.12.056>.

[65] M. Wang, M. Fang, X. Min, Z. Huang, C. Tang, Y. Liu, X. Wu, Molten salt synthesis of $\text{NaNb}_x\text{Ta}_{1-x}\text{O}_3$ perovskites with enhanced photocatalytic activity, *Chem. Phys. Lett.* 686 (2017) 18–25, <https://doi.org/10.1016/j.cplett.2017.08.029>.

[66] V. Senthil, T. Badapanda, A. Chithambaram, A. Chandra Bose, S. Panigrahi, Impedance spectroscopy and photocatalysis water splitting for hydrogen production with cerium modified $\text{SrBi}_2\text{Ta}_2\text{O}_9$ ferroelectrics, *Int. J. Hydrogen Energy* 41 (2016) 22856–22865, <https://doi.org/10.1016/j.ijhydene.2016.08.139>.

[67] Y. Li, G. Chen, H. Zhang, Z. Li, Photocatalytic water splitting of $\text{La}_2\text{AlTaO}_7$ and the effect of aluminum on the electronic structure, *J. Phys. Chem. Solids* 70 (2009) 536–540, <https://doi.org/10.1016/j.jpcs.2008.12.005>.

[68] H. Zhang, G. Chen, X. Li, Q. Wang, Electronic structure and water splitting under visible light irradiation of $\text{BiTa}_{1-x}\text{Cu}_x\text{O}_4$ ($x = 0.00\text{--}0.04$) photocatalysts, *Int. J. Hydrogen Energy* 34 (2009) 3631–3638, <https://doi.org/10.1016/j.ijhydene.2009.02.053>.

[69] T. Ishihara, H. Nishiguchi, K. Fukamachi, Y. Takita, Effects of acceptor doping to KTaO_3 on photocatalytic decomposition of pure H_2O , *J. Phys. Chem. B* 103 (1999) 1–3, <https://doi.org/10.1021/jp983590k>.

[70] R. Asai, H. Nemoto, Q. Jia, K. Saito, A. Iwase, A. Kudo, A visible light responsive rhodium and antimony-codoped SrTiO_3 powdered photocatalyst loaded with an IrO_2 cocatalyst for solar water splitting, *Chem. Commun. (Camb.)* 50 (2014) 2543–2546, <https://doi.org/10.1039/C3CC49279F>.

[71] Y. Ham, T. Hisatomi, Y. Goto, Y. Moriya, Y. Sakata, A. Yamakata, J. Kubota, K. Domen, Flux-mediated doping of SrTiO_3 photocatalysts for efficient overall water splitting, *J. Mater. Chem. A Mater. Energy Sustain.* 4 (2016) 3027–3033, <https://doi.org/10.1039/C5TA04843E>.

[72] J. Luo, P.A. Maggard, Hydrothermal synthesis and photocatalytic activities of SrTiO_3 -Coated Fe_2O_3 and BiFeO_3 , *Adv. Mater.* 18 (2006) 514–517, <https://doi.org/10.1002/adma.200500109>.

[73] H.W. Kang, S.N. Lim, S. Bin Park, Co-doping schemes to enhance H_2 evolution under visible light irradiation over $\text{SrTiO}_3\text{-Ni/M}$ (M = La or Ta) prepared by spray pyrolysis, *Int. J. Hydrogen Energy* 37 (2012) 5540–5549, <https://doi.org/10.1016/j.ijhydene.2012.01.007>.

[74] H.W. Kang, S. Bin Park, H_2 evolution under visible light irradiation from aqueous methanol solution on $\text{SrTiO}_3\text{-Cr/Ta}$ prepared by spray pyrolysis from polymeric precursor, *Int. J. Hydrogen Energy* 36 (2011) 9496–9504, <https://doi.org/10.1016/j.ijhydene.2011.05.094>.

[75] H. Kato, A. Kudo, Visible-light-response and photocatalytic activities of TiO_2 and SrTiO_3 photocatalysts codoped with antimony and chromium, *J. Phys. Chem. B* 106 (2002) 5029–5034, <https://doi.org/10.1021/jp0255482>.

[76] A.M. Huerta-Flores, L.M. Torres-Martínez, E. Moctezuma, Overall photocatalytic water splitting on $\text{Na}_2\text{Zr}_x\text{Ti}_{6-x}\text{O}_13$ ($x = 0, 1$) nanobelts modified with metal oxide nanoparticles as cocatalysts, *Int. J. Hydrogen Energy* 42 (2017) 14547–14559, <https://doi.org/10.1016/j.ijhydene.2017.04.203>.

[77] R. Wang, S. Ni, G. Liu, X. Xu, Hollow CaTiO_3 cubes modified by La/Cr co-doping for efficient photocatalytic hydrogen production, *Appl. Catal. B Environ.* 225 (2018) 139–147, <https://doi.org/10.1016/j.apcatb.2017.11.061>.

[78] J. Lv, T. Kako, Z. Li, Z. Zou, J. Ye, Synthesis and photocatalytic activities of NaNbO_3 rods modified by In_2O_3 , *Nanoparticles* (2010) 6157–6162.

[79] H. Iwakura, H. Einaga, Y. Teraoka, Relationship between cation arrangement and photocatalytic activity for Sr-Al-Nb-O double perovskite, *Inorg. Chem.* 49 (2010) 11362–11369, <https://doi.org/10.1021/ci101208q>.

[80] J. Li, J. Zeng, L. Jia, W. Fang, Investigations on the effect of $\text{Cu}^{2+}/\text{Cu}^{1+}$ redox couples and oxygen vacancies on photocatalytic activity of treated $\text{LaNi}_{1-x}\text{Cu}_x\text{O}_3$ ($x = 0.1, 0.4, 0.5$), *Int. J. Hydrogen Energy* 35 (2010) 12733–12740, <https://doi.org/10.1016/j.ijhydene.2010.08.140>.

[81] J. Li, L. Jia, W. Fang, J. Zeng, Enhancement of activity of $\text{LaNi}_{0.7}\text{Cu}_{0.3}\text{O}_3$ for photocatalytic water splitting by reduction treatment at moderate temperature, *Int. J. Hydrogen Energy* 35 (2010) 5270–5275, <https://doi.org/10.1016/j.ijhydene.2010.03.090>.

[82] Y. Li, G. Chen, H. Zhang, Z. Li, Electronic structure and photocatalytic water splitting of lanthanum-doped $\text{Bi}_2\text{AlNbO}_7$, *Mater. Res. Bull.* 44 (2009) 741–746, <https://doi.org/10.1016/j.materbull.2008.09.020>.

[83] Y. Li, Y. Huang, J. Wu, M. Huang, J. Lin, Photocatalytic activities for hydrogen evolution of new layered compound series $\text{HLaTa}_{x/3}\text{Nb}_{2-x/3}\text{O}_3/\text{Pt}$ ($x = 0, 2, 3, 4$, and 6), *J. Hazard. Mater.* 177 (2010) 458–464, <https://doi.org/10.1016/j.jhazmat.2009.12.055>.

[84] H. Jeong, T. Kim, D. Kim, K. Kim, Hydrogen production by the photocatalytic overall water splitting on $\text{NiO/Sr}_2\text{Ti}_2\text{O}_7$: Effect of preparation method, *Int. J. Hydrogen Energy* 31 (2006) 1142–1146, <https://doi.org/10.1016/j.ijhydene.2005.10.005>.

[85] C. Hu, H. Teng, Influence of structural features on the photocatalytic activity of NaTaO_3 powders from different synthesis methods, *Appl. Catal. A Gen.* 331 (2007) 44–50, <https://doi.org/10.1016/j.apcata.2007.07.024>.

[86] Y.C. Chiou, U. Kumar, J.C.S. Wu, Photocatalytic splitting of water on NiO/InTaO_4 catalysts prepared by an innovative sol-gel method, *Appl. Catal. A Gen.* 357 (2009) 73–78, <https://doi.org/10.1016/j.apcata.2009.01.016>.

[87] C.C. Hu, T.F. Yeh, H. Teng, Pyrochlore-like $\text{K}_2\text{Ta}_2\text{O}_6$ synthesized from different methods as efficient photocatalysts for water splitting, *Catal. Sci. Technol.* 3 (2013) 1798–1804, <https://doi.org/10.1039/c3cs00008g>.

[88] C.W. Lee, D.W. Kim, I.S. Cho, S. Park, S.S. Shin, S.W. Seo, K.S. Hong, Simple synthesis and characterization of SrSnO_3 nanoparticles with enhanced photocatalytic activity, *Int. J. Hydrogen Energy* 37 (2012) 10557–10563, <https://doi.org/10.1016/j.ijhydene.2012.04.063>.

[89] H. Kato, H. Kobayashi, A. Kudo, Role of Ag^+ in the band structures and photocatalytic properties of AgM_3 (M: Ta and Nb) with the perovskite structure, *J. Phys. Chem. B* 106 (2002) 12441–12447, <https://doi.org/10.1021/jp025974n>.

[90] A. Kudo, Y. Miseki, Heterogeneous photocatalyst materials for water splitting, *Chem. Soc. Rev.* 38 (2009) 253–278, <https://doi.org/10.1039/b800489g>.

[91] J. Ran, J. Zhang, J. Yu, M. Jaroniec, S.Z. Qiao, Earth-abundant cocatalysts for semiconductor-based photocatalytic water splitting, *Chem. Soc. Rev.* 43 (2014) 7787–7812, <https://doi.org/10.1039/c3cs60425j>.

[92] J. Shi, L. Guo, ABO_3 -based photocatalysts for water splitting, *Prog. Nat. Sci. Mater. Int.* 22 (2012) 592–615, <https://doi.org/10.1016/j.pnsc.2012.12.002>.

[93] D.-H. Wang, L. Wang, A.-W. Xu, Room-temperature synthesis of $\text{Zn}_{0.80}\text{Cd}_{0.20}\text{S}$ solid solution with a high visible-light photocatalytic activity for hydrogen evolution, *Nanoscale* 4 (2012) 2046–2053, <https://doi.org/10.1039/c2nr11972b>.

[94] T. Zhang, K. Zhao, J. Yu, J. Jin, Y. Qi, H. Li, X. Hou, G. Liu, Photocatalytic water splitting for hydrogen generation on cubic, orthorhombic, and tetragonal KNbO_3 microcubes, *Nanoscale* 5 (2013) 8375–8383, <https://doi.org/10.1039/c3nr02356g>.

[95] L. Wang, W. Wang, Photocatalytic hydrogen production from aqueous solutions over novel $\text{Bi}_{0.5}\text{Na}_{0.5}\text{TiO}_3$ microspheres, *Int. J. Hydrogen Energy* 37 (2012) 3041–3047, <https://doi.org/10.1016/j.ijhydene.2011.10.105>.

[96] D. Arney, L. Fuoco, J. Boltersdorf, P.A. Maggard, Flux synthesis of $\text{Na}_2\text{Ca}_2\text{Nb}_4\text{O}_{13}$: the influence of particle shapes, surface features, and surface areas on photocatalytic hydrogen production, *J. Am. Ceram. Soc.* 96 (2013) 1158–1162, <https://doi.org/10.1111/jace.12122>.

[97] H. Yoshida, M. Takeuchi, M. Sato, L. Zhang, T. Teshima, M.G. Chaskar, Potassium hexatitanate photocatalysts prepared by a flux method for water splitting, *Catal. Today* 232 (2014) 158–164, <https://doi.org/10.1016/j.cattod.2013.10.046>.

[98] D. Xu, S. Yang, Y. Jin, M. Chen, W. Fan, B. Luo, W. Shi, Ag-Decorated ATaO_3 (A = K, Na) Nanocube Plasmonic Photocatalysts with Enhanced Photocatalytic Water-Splitting Properties, *Langmuir* 31 (2015) 9694–9699, <https://doi.org/10.1021/acs.langmuir.5b01294>.

[99] Q. Zhang, Z. Li, S. Wang, R. Li, X. Zhang, Z. Liang, H. Han, S. Liao, C. Li, Effect of Redox Cocatalysts Location on Photocatalytic Overall Water Splitting over Cubic NaTaO_3 Semiconductor Crystals Exposed with Equivalent Facets, *ACS Catal.* 6 (2016) 2182–2191, <https://doi.org/10.1021/acscatal.6b02503>.

[100] C. Zhou, G. Chen, Y. Li, H. Zhang, J. Pei, Photocatalytic activities of $\text{Sr}_2\text{Ta}_2\text{O}_7$ nanosheets synthesized by a hydrothermal method, *Int. J. Hydrogen Energy* 34 (2009) 2113–2120, <https://doi.org/10.1016/j.ijhydene.2008.12.074>.

[101] N. Arai, N. Saito, H. Nishiyama, Y. Shimodaira, H. Kobayashi, Y. Inoue, K. Sato, Photocatalytic activity for overall water splitting of RuO_2 -loaded $\text{Y}_{x}\text{In}_{2-x}\text{O}_3$ ($x = 0.9\text{--}1.5$), *J. Phys. Chem. C* 112 (2008) 5000–5005, <https://doi.org/10.1021/jp709629t>.

[102] S.H. Kim, S. Park, C.W. Lee, B.S. Han, S.W. Seo, J.S. Kim, I.S. Cho, K.S. Hong, Photophysical and photocatalytic water splitting performance of stibiotantalite type-structure compounds, SbMO_4 (M = Nb, Ta), *Int. J. Hydrogen Energy* 37 (2012) 16895–16902, <https://doi.org/10.1016/j.ijhydene.2012.08.123>.

[103] L.M. Torres-Martínez, R. Gómez, O. Vázquez-Cuchillo, I. Juárez-Ramírez, A. Cruz-López, F.J. Alejandre-Sandoval, Enhanced photocatalytic water splitting hydrogen

production on $\text{RuO}_2/\text{La:NaTaO}_3$ prepared by sol-gel method, *Catal. Commun.* 12 (2010) 268–272, <https://doi.org/10.1016/j.catcom.2010.09.032>.

[104] B. Zielińska, E. Mijowska, R.J. Kalenczuk, Synthesis, characterization and photocatalytic properties of lithium tantalate, *Mater. Charact.* 68 (2012) 71–76, <https://doi.org/10.1016/j.matchar.2012.03.008>.

[105] C. Zeng, T. Hu, N. Hou, S. Liu, W. Gao, R. Cong, T. Yang, Photocatalytic pure water splitting activities for ZnGa_2O_4 synthesized by various methods, *Mater. Res. Bull.* 61 (2015) 481–485, <https://doi.org/10.1016/j.materresbull.2014.10.041>.

[106] M. Ni, M.K.H. Leung, D.Y.C. Leung, K. Sumathy, A review and recent developments in photocatalytic water-splitting using TiO_2 for hydrogen production, *Renewable Sustainable Energy Rev.* 11 (2007) 401–425, <https://doi.org/10.1016/j.rser.2005.01.009>.

[107] Z. Wu, G. Li, F. Zhang, W. Zhang, Photocatalytic activity of $\text{NaTaO}_3:\text{La}$ prepared under different atmospheres, *Appl. Surf. Sci.* 319 (2014) 372–375, <https://doi.org/10.1016/j.apsusc.2014.06.099>.

[108] S.M.A. Shibli, P.S. Arun, A.V. Raj, Exploration of octahedrally shaped MnCo_2O_4 catalyst particles for visible light driven photocatalytic water splitting reaction, *RSC Adv.* 5 (2015) 19393–19399, <https://doi.org/10.1039/c4ra12646g>.

[109] P. Wu, J. Shi, Z. Zhou, W. Tang, L. Guo, $\text{CaTaO}_2\text{N-CaZrO}_3$ solid solution: band-structure engineering and visible-light-driven photocatalytic hydrogen production, *Int. J. Hydrogen Energy* 37 (2012) 13704–13710, <https://doi.org/10.1016/j.ijhydene.2012.02.143>.

[110] X. Yu, X. An, A. Shavel, M. Ibáñez, A. Cabot, The effect of the Ga content on the photocatalytic hydrogen evolution of $\text{CuIn}_{1-x}\text{Ga}_x\text{S}_2$ nanocrystals, *J. Mater. Chem. A Mater. Energy Sustain.* 2 (2014) 12317–12322, <https://doi.org/10.1039/c4ta01315h>.

[111] W.J. Fan, Z.F. Zhou, W.B. Xu, Z.F. Shi, F.M. Ren, H.H. Ma, S.W. Huang, Preparation of ZnIn_2S_4 /fluoropolymer fiber composites and its photocatalytic H_2 evolution from splitting of water using Xe lamp irradiation, *Int. J. Hydrogen Energy* 35 (2010) 6525–6530, <https://doi.org/10.1016/j.ijhydene.2010.04.036>.

[112] W. Zhao, K. Maeda, F. Zhang, T. Hisatomi, K. Domen, Effect of post-treatments on the photocatalytic activity of $\text{Sm}_2\text{Ti}_2\text{S}_2\text{O}_5$ for the hydrogen evolution reaction, *Phys. Chem. Chem. Phys.* 16 (2014) 12051, <https://doi.org/10.1039/c3cp54668c>.

[113] H. Kato, A. Kudo, Water splitting into H_2 and O_2 on alkali tantalate photocatalysts ATaO_3 ($\text{A} = \text{Li, Na, and K}$), *J. Phys. Chem. B* 105 (2001) 4285–4292, <https://doi.org/10.1021/jp004386b>.

[114] H. Lee, Y. Park, M. Kang, Synthesis of characterization of $\text{Zn}_x\text{Ti}_y\text{S}$ and its photocatalytic activity for hydrogen production from methanol/water photo-splitting, *J. Ind. Eng. Chem.* 19 (2013) 1162–1168, <https://doi.org/10.1016/j.jiec.2012.12.013>.

[115] J. Shi, J. Ye, Q. Li, Z. Zhou, H. Tong, G. Xi, L. Guo, Single-Crystal Nanosheet-Based Hierarchical AgSbO_3 with Exposed {001} Facets: Topotactic Synthesis and Enhanced Photocatalytic Activity, *Chem. A Eur. J.* 18 (2012) 3157–3162, <https://doi.org/10.1002/chem.201102214>.

[116] H. Kato, A. Kudo, Photocatalytic reduction of nitrate ions over tantalate photocatalysts, *Phys. Chem. Chem. Phys.* 4 (2002) 2833–2838, <https://doi.org/10.1039/b110511f>.

[117] K.I. Shimizu, S. Itoh, T. Hatamachi, T. Kodama, M. Sato, K. Toda, Photocatalytic water splitting on ni-intercalated ruddlesden-popper tantalate $\text{H}_2\text{La}_{2/3}\text{Ta}_2\text{O}_7$, *Chem. Mater.* 17 (2005) 5161–5166, <https://doi.org/10.1021/cm050982c>.

[118] S. Ikeda, M. Fubuki, Y.K. Takahara, M. Matsumura, Photocatalytic activity of hydrothermally synthesized tantalate pyrochlorites for overall water splitting, *Appl. Catal. A Gen.* 300 (2006) 186–190, <https://doi.org/10.1016/j.apcata.2005.11.007>.

[119] J. Cai, Y. Zhu, D. Liu, M. Meng, Z. Hu, Z. Jiang, Synergistic effect of titanate-anatase heterostructure and hydrogenation-induced surface disorder on photocatalytic water splitting, *ACS Catal.* 5 (2015) 1708–1716, <https://doi.org/10.1021/acscatal.5b00055>.

[120] H. Kato, H. Kobayashi, A. Kudo, Role of Ag^+ in the band structures and photocatalytic properties of AgMO_3 (M: Ta and Nb) with the perovskite structure, *J. Phys. Chem. B* 106 (2002) 12441–12447, <https://doi.org/10.1021/jp025974n>.

[121] Z.G. Yi, J.H. Ye, Band gap tuning of $\text{Na}_{1-x}\text{La}_x\text{Ta}_{1-x}\text{Cr}_x\text{O}_3$ for H_2 generation from water under visible light irradiation, *J. Appl. Phys.* 106 (2009) 074910, , <https://doi.org/10.1063/1.3243282>.

[122] H. Husin, H.M. Chen, W.N. Su, C.J. Pan, W.T. Chuang, H.S. Sheu, B.J. Hwang, Green fabrication of La-doped NaTaO_3 via H_2O_2 assisted sol-gel route for photocatalytic hydrogen production, *Appl. Catal. B Environ.* 102 (2011) 343–351, <https://doi.org/10.1016/j.apcatb.2010.12.024>.

[123] H. Husin, W.-N. Su, H.-M. Chen, C.-J. Pan, S.-H. Chang, J. Rick, W.-T. Chuang, H.-S. Sheu, B.-J. Hwang, Photocatalytic hydrogen production on nickel-loaded $\text{La}_x\text{Na}_{1-x}\text{TaO}_3$ prepared by hydrogen peroxide-water based process, *Green Chem.* 13 (2011) 1745–1754, <https://doi.org/10.1039/c1gc15070g>.

[124] A. Iwase, H. Kato, A. Kudo, The effect of alkaline earth metal ion dopants on photocatalytic water splitting by NaTaO_3 powder, *ChemSusChem.* 2 (2009) 873–877, <https://doi.org/10.1002/cssc.200900160>.

[125] H. Kato, A. Kudo, Water splitting into H_2 and O_2 on alkali tantalate photocatalysts ATaO_3 ($\text{A} = \text{Li, Na, and K}$), *J. Phys. Chem. B* 105 (2001) 4285–4292, <https://doi.org/10.1021/jp004386b>.

[126] A. Molak, M. Pilch, Visible light absorbance enhanced by nitrogen embedded in the surface layer of Mn-doped sodium niobate crystals, detected by ultra violet -Visible spectroscopy, x-ray photoelectron spectroscopy, and electric conductivity tests, *J. Appl. Phys.* 119 (2016) 204901, , <https://doi.org/10.1063/1.4948937>.

[127] B. Modak, S.K. Ghosh, An efficient strategy for controlled band gap engineering of KTaO_3 , *J. Phys. Chem. C.* 120 (2016) 6920–6929, <https://doi.org/10.1021/acs.jpcc.5b11777>.

[128] T. Takata, K. Domen, Development of non-oxide semiconductors as light harvesting materials in photocatalytic and photoelectrochemical water splitting, *Dalton Trans.* 46 (2017) 10529–10544, <https://doi.org/10.1039/c7dt00867h>.

[129] S. Irfan, Y. Shen, S. Rizwan, H.-C. Wang, S.B. Khan, C.-W. Nan, Band-Gap Engineering and Enhanced Photocatalytic Activity of Sm and Mn Doped BiFeO_3 Nanoparticles, *J. Am. Ceram. Soc.* 100 (2017) 31–40, <https://doi.org/10.1111/jace.14487>.